TECHNICAL REPORT STANDARD TITLE PAGE

1. Report No.	2. Government Accession No.	3. Recipient's Catalog No.
DOT/FAA-PS-89/5		

4. Title and Subtitle	5. Report Date
Dual-Beam Autocorrelation Based Wind Estimates from Airport Surveillance Radar Signals	21 June 1989
	6. Performing Organization Code
7. Author(s)	8. Performing Organization Report No.
Mark E. Weber	ATC-167
9. Performing Organization Name and Address	10. Work Unit No. (TRAIS)
Lincoln Laboratory, MIT P.O. Box 73 Lexington, MA 02173-0073	11. Contract or Grant No. DTFA-01L-83-4-10579
12. Sponsoring Agency Name and Address	13. Type of Report and Period Covered
Department of Transportation Federal Aviation Administration 800 Independence Avenue, SW Washington, DC 20591	Project Report
	14. Sponsoring Agency Code

15. Supplementary Notes

The work reported in this document was performed at Lincoln Laboratory, a center for research operated by Massachusetts Institute of Technology, under Air Force Contract F19628-85-C-0002.

16. Abstract

This report describes an efficient, autocorrelation based algorithm for estimating low altitude radial winds using signals from the two receiving beams of an airport surveillance radar (ASR). The approach seeks to achieve the accuracy demonstrated previously for spectral domain dual beam velocity estimators with significantly reduced computational requirements. Fundamental to the technique is the assumption that the power spectrum measured with an airport surveillance radar's broad elevation beam can be fitted by a two component Gaussian model. The parameters of this model are estimated using measured low-order autocorrelation lags from the low and high beam received signals. The desired near surface radial velocity estimate is obtained directly as one of these parameters — the center frequency of the low altitude Gaussian spectrum component.

Simulated data and field measurements from Lincoln Laboratory's experimental ASR-8 in Huntsville, Alabama were used to evaluate the accuracy of the autocorrelation based velocity estimates. Monto Carlo simulations indicate that biases relative to the near surface outflow velocity in a microburst would be less than 2.5 m/s unless the microburst were distant (range > 12 km) or very shallow (depth of maximum wind speed layer < 50 m). Estimate standard deviations averaged 0.5 m/s after the spatial filtering employed in our processing sequence. The algorithm's velocity estimate accuracy was sufficient to allow for automatic detection of measured microbursts during 1988 with a detection probability exceeding 0.9 and a false alarm probability less than 0.05. Our analysis indicates that the dual-beam autocorrelation based velocity estimator should support ASR wind shear detection at approximately the same level of confidence as the low-high beam spectral differencing algorithm evaluated by Weber and Noyes (1988).

17. Key Words	18. Distribution Statement
microburst low altitude wind shear airport surveillance radar velocity estimation parameter-based spectral estimation	Document is available to the public through the National Technical Information Service, Springfield, VA 22161.

19. Security Classif. (of this report)	20. Security Classif. (of this page)	21. No. of Pages	22. Price
Unclassified	Unclassified	60	

FORM DOT F 1700.7 (8-72) Reproduction of completed page authorized

Dual-Beam Autocorrelation Based Wind Estimates from Airport Surveillance Radar Signals

ABSTRACT

This report describes an efficient, autocorrelation based algorithm for estimating low altitude radial winds using signals from the two receiving beams of an airport surveillance radar (ASR). The approach seeks to achieve the accuracy demonstrated previously for spectral domain dual beam velocity estimators with significantly reduced computational requirements. Fundamental to the technique is the assumption that the power spectrum measured with an airport surveillance radar's broad elevation beam can be fitted by a two component Gaussian model. The parameters of this model are estimated using measured low-order autocorrelation lags from the low and high beam received signals. The desired near surface radial velocity estimate is obtained directly as one of these parameters -- the center frequency of the "low altitude" Gaussian spectrum component.

Simulated data and field measurements from Lincoln Laboratory's experimental ASR-8 in Huntsville, Alabama were used to evaluate the accuracy of the autocorrelation based velocity estimates. Monte Carlo simulations indicate that biases relative to the near surface outflow velocity in a microburst would be less than 2.5 m/s unless the microburst were distant (range $>$ 12 km) or very shallow (depth of maximum wind speed layer $<$ 50 m). Estimate standard deviations averaged 0.5 m/s after the spatial filtering employed in our processing sequence. The algorithm's velocity estimate accuracy was sufficient to allow for automatic detection of measured microbursts during 1988 with a detection probability exceeding 0.9 and a false alarm probability less than 0.05. Our analysis indicates that the dual-beam autocorrelation based velocity estimator should support ASR wind shear detection at approximately the same level of confidence as the low-high beam spectral differencing algorithm evaluated by Weber and Noyes (1988).

TABLE OF CONTENTS

Abstract iii

List of Illustrations vii

List of Tables ix

I. INTRODUCTION 1

II. VELOCITY ESTIMATION BASED ON A DUAL GAUSSIAN SPECTRUM SHAPE MODEL 5

A. Velocity Spectra in Microburst Cores 5

B. Autocorrelation Based Dual Gaussian Fits to the Measured Spectra 8

1. Estimates Using $R(\tau)$ and $R(2\tau)$ 8

2. Estimates Using $R(0)$ and $R(\tau)$ 11

III. EVALUATION OF VELOCITY ESTIMATES USING SIMULATIONS AND FIELD MEASUREMENTS 13

A. Velocity Estimates using Simulated ASR Signals 13

B. Field Measurements from Huntsville Experimental ASR 25

IV. DISCUSSION AND FUTURE WORK 37

REFERENCES 39

APPENDIX A: ESTIMATION OF DUAL GAUSSIAN SPECTRAL PARAMETERS USING $R(\tau)$ and $R(2\tau)$ 41

APPENDIX B: ESTIMATION OF DUAL GAUSSIAN SPECTRAL PARAMETERS USING $R(0)$ and $R(\tau)$ 43

APPENDIX C: SIMULATION OF AIRPORT SURVEILLANCE RADAR SIGNALS FROM MICROBURSTS 44

LIST OF ILLUSTRATIONS

Figure No.	Title	Page
II-1	Velocity spectra measured with ASR in approaching (left) and receding (right) radial velocity cores of example microbursts. The ordinate is relative power in linear units. Spectra are plotted for both low (solid) and high (dashed) beam signals. Dashed vertical lines show mean velocities measured by pencil beam radar at 0.7 degrees elevation at same locations and times.	6
II-2	Velocity spectra reconstructed from ASR autocorrelation lag measurements in approaching (left) and receding (right) radial velocity cores of microbursts. The spectral model of equation (1) was used with parameters estimated from $R(\tau)$ and $R(2\tau)$ as described in Appendix A. The microburst examples and plot format are as in Figure III-1.	9
III-1	Spectral differencing and autocorrelation based velocity estimate bias and standard deviation versus "true" outflow velocity. The velocity model of Figure III-2 is scaled proportionally to the abscissae. Solid, dashed and chain dashed curves for standard deviation pertain respectively to single resolution cell estimates, estimates after spatial median filtering and after Gaussian smoothing along the range axis.	14
III-2	Model vertical profiles of radial velocity, reflectivity and spectrum width in approaching portion of a microburst.	17
III-3	Spectral differencing and autocorrelation based velocity estimate bias and standard deviation versus outflow reflectivity. The velocity model of Figure III-2 is assumed. The curve for standard deviation pertains to estimates after spatial median filtering followed by Gaussian smoothing along the range axis.	19
III-4	Spectral differencing and autocorrelation based velocity estimate bias and standard deviation versus outflow height. The velocity model of Figure III-2 is scaled proportionally to the lower abscissa labels. The curve for standard deviation pertains to estimates after spatial median filtering followed by Gaussian smoothing along the range axis.	21
III-5	Simulated microburst radial velocity versus range measurements from an ASR. The solid sinusoid is the model for the surface radial wind associated with the microburst. Dashed and chain dashed curves represent estimates using the spectral differencing and autocorrelation based algorithms. The upper plot simulates single resolution cell estimates: the lower plot includes the spatial filtering described in the text.	22

III-6 Images of the radial velocity field in a microburst producing thunderstorm near Huntsville, Alabama on 15 August 1988. The upper left panel shows measurements from the MIT C-band beam weather radar scanning in PPI mode at 0.6° elevation angle. Upper right panel is field estimated from ASR signals using the spectral differencing method. Lower left panel is corresponding field from autocorrelation based algorithm. Lower right panel uses autocorrelation based algorithm and high and low beam signals collected on different antenna scans. 27

III-7 Images of the radial velocity field in a microburst producing thunderstorm near Huntsville, Alabama on 21 June 1988. The upper panel shows measurements from the MIT C-band beam weather radar scanning in PPI mode at 0.6° elevation angle. Lower right panel is field estimated from ASR signals using the spectral differencing method. Lower left panel is corresponding field from autocorrelation based algorithm. 29

III-8 Images of the radial velocity field in a microburst producing thunderstorm near Huntsville, Alabama on 24 June 1988. The upper panel shows measurements from the MIT C-band beam weather radar scanning in PPI mode at 0.6° elevation angle. Lower right panel is field estimated from ASR signals using the spectral differencing method. Lower left panel is corresponding field from autocorrelation based algorithm. 31

III-9 Images of radial velocity field in a microburst producing thunderstorm near Huntsville, Alabama on 25 June 1988. The upper panel shows measurements from the MIT C-band beam weather radar scanning in PPI mode at 0.6° elevation angle. Lower right panel is field estimated from ASR signals using the spectral differencing method. Lower left panel is corresponding field from autocorrelation based algorithm. 33

C-1 Simulated underlying ASR power spectra for microburst wind field model of Figure III-2 (and its mirror image). Plot format is as in Figures II-1 and II-2. 45

C-2 Simulated three-degree-of-freedom ASR power spectra estimates. Underlying spectra are as in Figure C-1. 46

C-3 Spectral differencing and autocorrelation based velocity estimate bias and standard deviation versus "true" outflow velocity. The simulations used here reproduce the alternating PRF waveform of an ASR-9 and the use of a four-coefficient interpolation filter. Plot format is as in Figure III-1. 48

LIST OF TABLES

Table No.	Title	Page
II-1	Microburst velocity shear estimates using spectral differencing and $R(\tau)$, $R(2\tau)$ dual Gaussian fit.	11
II-2	Microburst velocity shear estimates using $R(0)$, $R(\tau)$ dual Gaussian fit.	12
III-1	Microburst detection algorithm performance for ASR-based velocity fields.	35

Dual-Beam Autocorrelation Based Wind Estimates from Airport Surveillance Radar Signals

I. INTRODUCTION

This report evaluates an efficient, autocorrelation based algorithm for estimating low altitude radial winds using signals from the two receiving beams of an airport surveillance radar (ASR). The described approach seeks to achieve the accuracy demonstrated previously for spectral domain dual beam velocity estimators (Anderson,1989; Atlas,1987,1989; Weber and Noyes,1988) with significantly reduced computational requirements.

The feasibility of a data processing augmentation to existing ASRs that would allow for detection of low altitude wind shear has been under investigation by Lincoln Laboratory and cooperating universities since 1984. This capability would require:

(a) a signal processing module that would suppress ground clutter and estimate the radial velocity of *near-surface* precipitation wind tracers;

(b) an algorithm to automatically recognize significant wind shear in the resulting velocity field.

Anderson (1987), Weber and Moser (1987) and Weber (1987) considered the impact of ground clutter on ASR wind measurements. Simulations and analysis of real clutter data from airport surveillance radars indicated that wind measurements were feasible even at short range provided that the reflectivity factor of the precipitation tracers was approximately 20 dBz or greater. Even when this condition is met however, accurate low-altitude radial wind estimates may not be obtained with "conventional" mean Doppler estimators when the radial wind component varies rapidly with altitude. In this situation, an ASR's fan-shaped elevation beam intercepts scatterers moving at both the near-surface velocity and the velocity of wind aloft; the result is a broad, possibly multi-modal velocity spectrum whose power-weighted mean differs markedly from the near surface radial wind velocity. Since both microbursts and gust fronts exhibit strong vertical shear in the horizontal winds near the ground, this beam resolution issue is of obvious importance.

Weber and Noyes (1988) used data from an experimental ASR operated during periods of nearby thunderstorm activity to evaluate three methods for estimating low altitude winds from ASR signals:

(i) high-pass filtering to exploit the fact that microburst outflow winds are often higher in absolute magnitude than winds aloft;

(ii) comparison of the strength of divergence regions detected in velocity fields from the high and low receiving beams of the ASR to "correct" the measured velocity shear values;

(iii) resolution cell by cell comparison of the power spectra of the low and high receiving beams to determine the velocity domain associated with near surface scatterers.

Our assessment included an end-to-end data processing evaluation whereby wind fields estimated from the ASR signals were passed into a slightly modified version of the Terminal Doppler Weather Radar's (TDWR) surface outflow detection algorithm (Merritt, 1987). The resulting microburst alarms were scored on a scan-by-scan basis against "truth" as determined from manual examination of wind fields measured with a colocated pencil-beam Doppler weather radar. Overall, the third method above -- transformation of high and low beam signals into the frequency domain followed by spectral differencing -- produced better detection performance (higher probability of detection and lower false alarm probability) and more accurate velocity shear estimates than the other two methods evaluated.

Use of this dual-beam signal processing approach, however, raises several implementation issues. ASRs normally transmit circularly polarized (CP) signals during heavy rain in order to reduce precipitation clutter in the aircraft detection processor. In order to avoid a resulting 15 to 20 dB loss in received power from weather echoes, any weather processor on an airport surveillance radar should receive its input from the opposite-sense polarized antenna port. ASR-8's and ASR-9's have only one path through the rotary joint for opposite sense polarized signals; thus during operation with circular polarization, weather data from both high and low beams could not be accessed simultaneously. Power spectra for the two beams would have to be calculated on alternate antenna scans, requiring memory storage for all data from one of the scans. Assuming range coverage to 20 km and two byte integer representation of the in-phase and quadrature signals, this would require 3 Mbytes of dedicated physical memory.

Another issue is the computational requirement of estimating power spectra for the two beams in each resolution cell and calculating a velocity based on the difference of the two spectra. Assuming that the spectra were estimated using Fast Fourier Transforms (FFT), about 1000 floating point operations per resolution cell would be required. For the same 20 km range coverage considered previously, this translates to 17 million floating point operations per second. While both the memory storage and processing speed requirements could be met, they would certainly drive the cost of the signal processing computer higher.

A third issue arises from the large variance and coarse quantization of power spectrum estimates obtained from a rapidly scanning airport surveillance radar. As implemented by Weber and Noyes (1988), the low and high beam power spectrum estimates were calculated from 34 successive pulses (2.6° in azimuth) and incoherently averaged over three successive range gates (360 m). Velocity resolution was about 2 m/s and the 90% confidence interval of the spectral estimates was 7 dB. Monte Carlo simulations indicate that the standard deviation of mean velocity estimates using our implementation is approximately 2 m/s. Thus additional spatial filtering had to be applied to the velocity field in order to achieve acceptable performance from the microburst detection algorithm.

In this report, we evaluate an alternative dual-beam velocity estimation technique that significantly reduces both memory storage and computational requirements. The basic strategy is to estimate the parameters of an assumed bimodal Gaussian power spectra, based on low-order autocorrelation lags from the low and high beam received signals. The desired low-altitude velocity estimate is then obtained directly as the center frequency of one of the two components of this spectral model. Because only the zero and one sample delay autocorrelation lags for each beam are used, physical memory storage requirements would be reduced to 0.5 Mbyte. Computational requirements are about 2 million floating point

operations per second. Estimate standard deviations of 2 m/s can be achieved without the need for range smoothing as required for the spectral differencing approach.

Section II describes the double Gaussian spectral model and algorithms for estimating its parameters from autocorrelation function measurements. This discussion draws heavily on measured microburst power spectra from our experimental ASR. In Section III, we evaluate the performance of the algorithm, using simulated and measured ASR signals from microbursts. Automatic microburst detection performance using this method and the spectral differencing approach evaluated by Weber and Noyes (1988) is compared statistically for our 1988 field measurements. Over the evaluated data set, the two methods provide similar performance. Section IV summarizes our findings and describes ongoing work.

II. VELOCITY ESTIMATION BASED ON A DUAL GAUSSIAN SPECTRUM SHAPE MODEL

A. Velocity Spectra in Microburst Cores

Figure II-1 shows examples of velocity spectra measured with our experimental airport surveillance radar in the cores of eight "wet" microbursts near Huntsville, Alabama. The spectra were estimated from FFTs of 34-sample Hamming windowed data sequences, incoherently averaged over three contiguous range gates. An adaptively-selected clutter filter (Weber,1987) was applied to the signals prior to Fourier transformation; in most of the examples shown, however, the reflectivity factor in the microburst core was sufficiently high that no filtering was required. Although our experimental radar transmitted pulses at a uniform repetition frequency (PRF), the eight/ten-pulse alternating PRF sequence to be used by ASR-9s could be accommodated by preceding the clutter filters with a shift-variant interpolation filter as described by Weber (1987).

The plots show calcuated spectra for both high (dashed) and low (solid) receiving beams. The left hand panels are for the approaching radial velocity cores of the microbursts and those in the right column are for the receding cores. The spectra have been normalized so that the areas under the curves are equal. For reference, radial velocities measured by the pencil beam weather radar at the same range-azimuth locations and times are indicated by dashed vertical lines. The pencil beam radar was scanned at 0.6^{o} elevation angle to estimate the near surface radial wind speed.

As discussed in Weber and Noyes (1988) the broad width and multimodal nature of these power spectra result in significant differences between the "true" near surface radial velocity and the ASR-based measurement when a conventional mean Doppler estimator is used. The discrepancy results, of course because the applicability of the mean Doppler estimate rests on the assumption of narrow-width, roughly symmetric power spectral shape. Of the displayed power spectra, only those in the approaching core on 1 August exhibit symmetry. The remaining spectra are strongly skewed and/or bi- or multi-modal. Some of this complexity arises from spectral estimate variance (recall that our procedure results in a 7 dB 90% confidence interval). As illustrated in Appendix C however, the dominant features of the spectra can be attributed to the interaction of an ASR's fan-shaped elevation beam with the strongly sheared radial wind field in an a microburst outflow.

Note that the low beam power spectral density always exceeds that of the high beam near the indicated surface wind speed. This reflects reduced high beam antenna gain near the surface, and is the basis for the spectral differencing technique alluded to above.

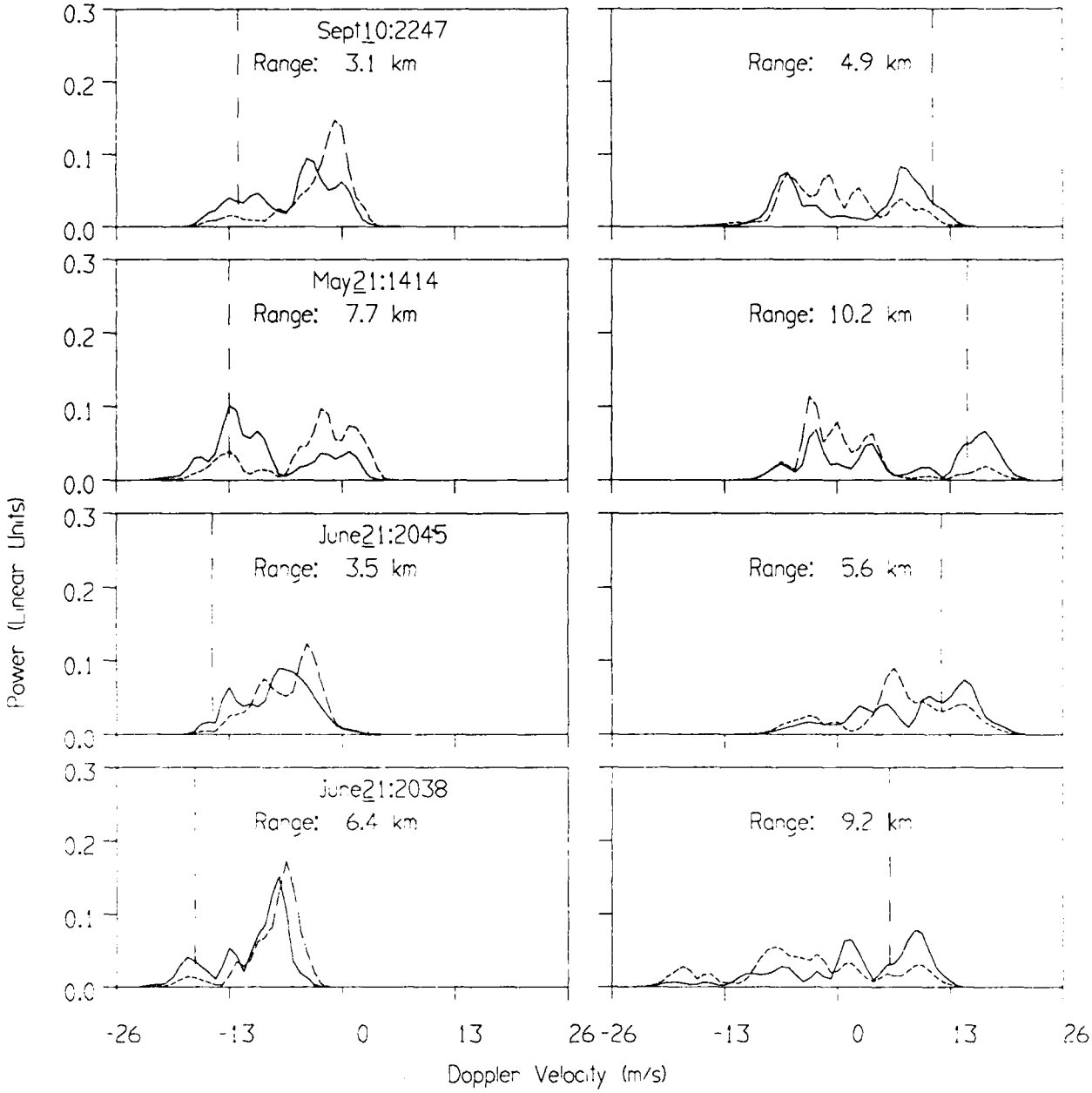

Figure II-1. Velocity spectra measured with ASR in approaching (left) and receding (right) radial velocity cores of example microbursts. The ordinate is relative power in linear units. Spectra are plotted for both low (solid) and high (dashed) beam signals. Dashed vertical lines show mean velocities measured by pencil beam radar at 0.7 degrees elevation at same locations and times.

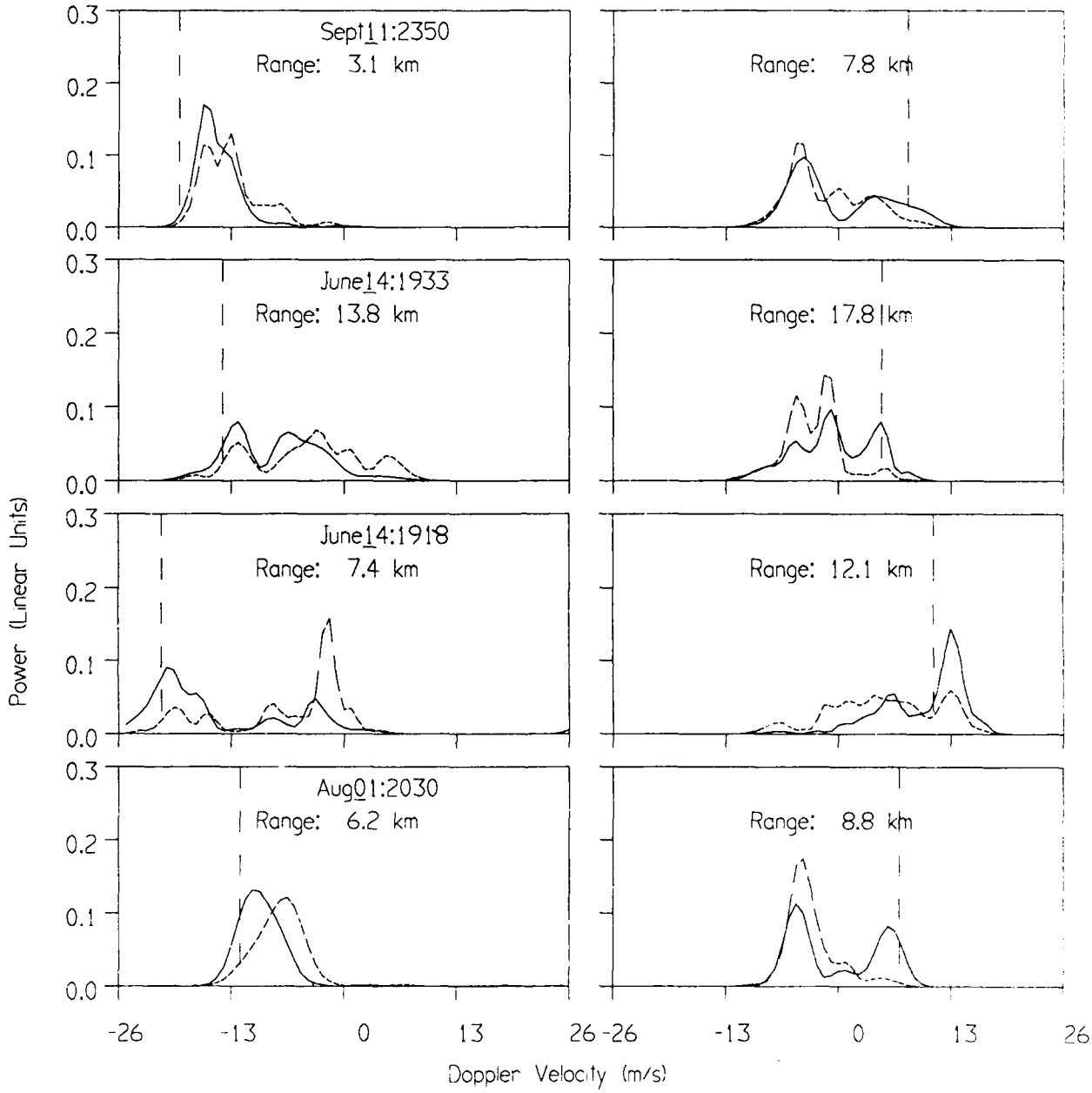

Figure II-1. (continued)

B. Autocorrelation Based Dual Gaussian Fits to the Measured Spectra

I. Estimates Using $R(\tau)$ and $R(2\tau)$

Examination of the above measured spectra suggests that the parameters of a double Gaussian power spectrum model might provide a better estimate of the low altitude wind field than the conventional mean Doppler method. Physically, the presence of two separated modes in the power spectra implies a radial velocity field that is strongly discontinuous within the radar's beamwidth, as at the top of a shallow microburst outflow. In a region where the radial wind speed varies linearly with height or is constant, the double Gaussian model can also adequately represent the power spectrum that would be measured by an ASR since the two components may overlap substantially, producing a broad, unimodal spectrum.

We assume therefore that the weather echo power spectra measured by the fan shaped elevation beam of an ASR can be approximately represented as:

$$S_i(f) = \frac{a_{i,1}}{\sqrt{2\pi}\sigma_1}\exp[\frac{-(f-f_1)^2}{2\sigma_1^2}] + \frac{a_{i,2}}{\sqrt{2\pi}\sigma_2}\exp[\frac{-(f-f_2)^2}{2\sigma_2^2}] \qquad (1)$$

where i=1,2 indexes the low and high receiving beams. The center frequencies and widths of the two spectral components are assumed to be identical between the two beams but the amplitudes will differ owing to the different weightings from the antenna patterns.

Appendix A describes a method of estimating the eight parameters in equations (1) using measurements of the low and high beam autocorrelation functions at lags τ and 2τ. The solution is constructed using knowledge of the beam patterns so that the parameters $a_{i,1}$, σ_1 and f_1 represent the spectral component associated with scatterers at low elevation angle. Figure II-2 plots the resulting dual Gaussian power spectra for the microburst cores shown previously. Although these are not optimum dual Gaussian fits to the measured spectra (for example, in a least squares sense) they generally correspond well to the data.

Low altitude velocity estimates can be derived from the calculated spectral parameters by reconstructing the spectra and implementing a low-high beam differencing algorithm as described in Weber and Noyes (1988). Table II-1 compares the resulting velocity shear estimates for these eight microbursts to those measured by the pencil beam "truth" radar and to those calculated using the spectral differencing technique applied directly to the measured power spectra. In seven of the eight cases considered, both ASR-based velocity shear estimates are in good agreement with the pencil beam measurements. For the spectra measured on 9-11-87, dual Gaussian fitting resulted in a substantially larger wind shear estimate than given by the pencil beam weather radar and the spectral differencing technique; this produced the larger overall RMS error associated with the dual Gaussian approach.

The above results indicate that the fidelity of the dual Gaussian spectral model to the measured signal characteristics may be sufficient to generate a reliable low altitude velocity estimate from ASR data. However, the described solution is not computationally efficient. Calculation of the first and second autocorrelation lags requires 1.5 times as many operations as would be needed to estimate $R(0)$ and $R(\tau)$. More importantly, the double Gaussian spectral parameters are determined iteratively (Appendix A), followed by numerical integration to derive a velocity

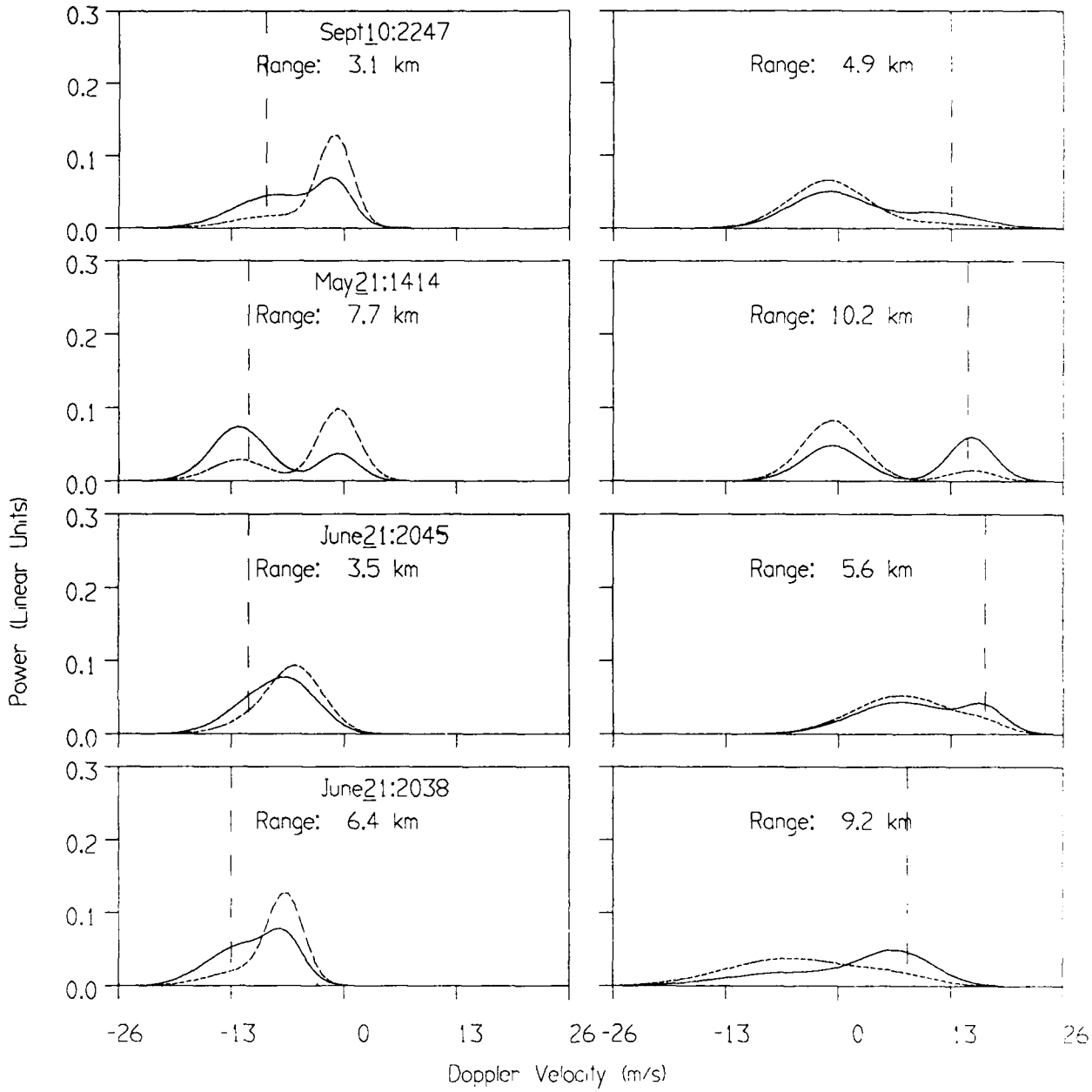

Figure II-2. Velocity spectra reconstructed from ASR autocorrelation lag measurements in approaching (left) and receding (right) radial velocity cores of microbursts. The spectral model of equation (1) was used with parameters estimated from $R(\tau)$ and $R(2\tau)$ as described in Appendix A. The microburst examples and plot format are as in Figure III-1.

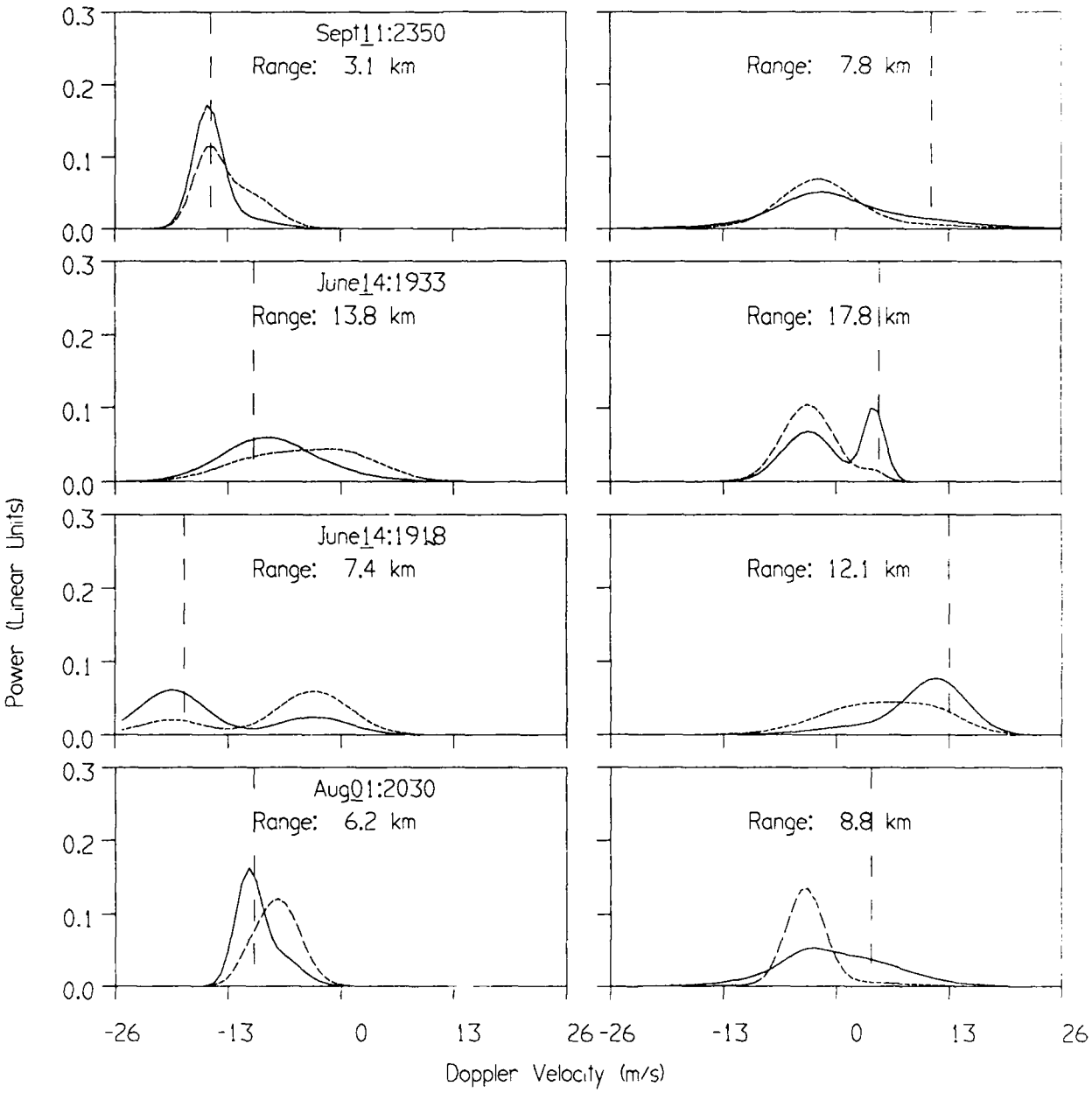

Figure II-2. (continued)

Table II-1: Microburst Velocity Shear Estimates Using Spectral Differencing and $R(\tau)$, $R(2\tau)$ Dual Gaussian Fit			
Date/Time	Pencil Beam Radar ΔV (m/s)	ASR Spectral Differencing (Measured)	ASR Spectral Differencing (Dual Gaussian Fit)
9-10-87 22:47	23	21	23
5-21-87 14:14	28	28	27
6-21-87 20:45	27	29	30
6-21-87 20:38	23	23	22
9-11-87 23:50	24	25	32
6-14-87 19:33	19	15	16
6-14-87 19:18	32	33	32
8-1-87 20:30	19	17	22
Average $\frac{\Delta V_{ASR}}{\Delta V_{TRUE}}$		0.96	1.05
RMS Relative Difference ΔV_{ASR} vs. ΔV_{TRUE}		0.09	0.15

estimate. In the following section we describe an approximate solution for the dual Gaussian parameters that leads to an efficient velocity estimation algorithm.

II. Estimates Using $R(0)$ and $R(\tau)$

The number of unknowns in equations (1) can be reduced from eight to six by assuming that the ratio of high and low beam amplitudes for each spectral component can be determined from a known beam weighting function, $w_{i,j}$:

$$S_i(f) = w_{i,1}\frac{a_1}{\sqrt{2\pi}\sigma_1}\exp[\frac{-(f-f_1)^2}{2\sigma_1^2}] + w_{i,2}\frac{a_2}{\sqrt{2\pi}\sigma_2}\exp[\frac{-(f-f_2)^2}{2\sigma_2^2}] \tag{2}$$

Appendix B describes a solution for the six spectral parameters using measurements of $R(0)$ and $R(\tau)$ in the two receiving beams of an ASR. The important result is that the center frequency of the "low altitude induced" spectral component can be derived as:

$$f_1 = \frac{1}{2\pi\tau}\tan^{-1}[R_1(\tau) - \frac{R_1(0)}{R_2(0)}\frac{w_{1,2}}{w_{2,2}}R_2(\tau)] \tag{3}$$

Thus if this center frequency can be shown to accurately represent the low altitude wind field, the ASR velocity estimation algorithm could be simplified to a standard pulse pair estimate, preceded by linear combination of the low and high beam autocorrelation estimates. This method was in fact proposed by Weber and Moser (1987) although we indicated there that better performance would be expected if the high and low beam signals were "orthogonalized" through linear combination of their in-phase and quadrature components prior to calculation of autocorrelation lags.

As described in Appendix B, the precomputed beam weights $w_{i,j}$ in equation (3) can be parameterized by an upper elevation angle (corresponding to the height of a microburst outflow) for the low altitude spectral component. In this report we will treat this angle as range independent, although better performance might be expected were it a decreasing function of range. For the microbursts treated previously, Table II-2 compares velocity shear estimates from equation (3) with those from the pencil beam weather radar. Upper elevation angles, θ_0 of 1°, 2° and 3°

were used in computing the $w_{i,j}$.

Table II-2: Microburst Velocity Shear Estimates Using $R(0)$, $R(\tau)$ Dual Gaussian Fit				
Date/Time	Pencil Beam Radar ΔV (m/s)	ASR ($\theta_0 = 3^0$)	ASR ($\theta_0 = 2^0$)	ASR ($\theta_0 = 1^0$)
9-10-87 22:47	23	13	18	26
5-21-87 14:14	28	26	31	36
6-21-87 20:45	27	20	22	28
6-21-87 20:38	23	18	22	27
9-11-87 23:50	24	17	19	25
6-14-87 19:33	19	12	16	22
6-14-87 19:18	32	33	36	39
8-1-87 20:30	19	14	18	25
Average $\frac{\Delta V_{ASR}}{\Delta V_{TRUE}}$		0.76	0.91	1.20
RMS Relative Difference ΔV_{ASR} vs. ΔV_{TRUE}		0.27	0.15	0.19

Note that as θ_0 is decreased, the weight $w_{1,2}/w_{2,2}$ increases (see Appendix B). When wind speed decreases with altitude as is normally the case in a microburst, the magnitude of the phase angle of the high beam's $R(\tau)$ autocorrelation lag will be smaller than that of the low beam. A simple vector construction illustrates that these observations account for the observed inverse relationship between θ_0 and the magnitude of the velocity shear estimate from equation (3).

Since the heights of microburst outflow winds vary considerably and since the above events were at different ranges from the radar, the "best" value for θ_0 was variable; indeed in many of these microbursts the best velocity measure for the approaching core corresponded to a different value for θ_0 than that for the receding core. Over the eight events however, weights $w_{i,j}$ computed using a value of 2° for θ_0 resulted in a shear estimates that on average were closest to those measured by the pencil beam radar; the corresponding RMS relative error was likewise minimum for this setting. While the match to the pencil beam radar measurements could have been improved by selecting a θ_0 slightly less than 2.0, we felt that such fine tuning was unwarranted given the small number of events used for the evaluation.

Comparison of Tables II-1 and II-2 suggests that the simple velocity estimator of equation (3) might provide comparable accuracy to the less constrained approach discussed in the previous subsection, provided that a suitable weight $w_{1,2}/w_{2,2}$ were selected. The following section examines the extent to which a single value for this weight would provide acceptable velocity estimates for a much larger data set than evaluated above.

III. EVALUATION OF VELOCITY ESTIMATES USING SIMULATIONS AND FIELD MEASUREMENTS

This section compares ASR radial velocity estimates from equation (3) to those derived from the full spectral differencing technique and to "truth" as defined from microburst models (part A) or simultaneous measurements from the pencil beam weather radar (part B). The data processing sequence involves the elements described in Weber (1987) and Weber and Noyes (1988):

(i) clutter-map based high pass filtering of 34 sample sequences from the high and low receiving beams;

(ii) velocity estimation using equation (3) or the spectral differencing algorithm described by Weber and Noyes (1988). For the autocorrelation based method, beam weights $w_{i,j}$ were calculated with θ_0 set to 2.0^o;

(iii) nine-point nearest neighbor spatial median filtering of the velocity field followed by smoothing along the range axis with a five-point Gaussian filter;

(iv) divergence detection using the surface outflow portion (Merritt, 1987) of the TDWR microburst detection algorithm.

All data used in part B were collected during 1988 in wet microbursts near Huntsville, Alabama. We note that the value of θ_0 used in calculating the weighting coefficient $w_{1,2}/w_{2,2}$ was derived from independent microburst data collected during 1987 as described in the preceding section.

A. Velocity Estimates using Simulated ASR Signals

As a function of "true" surface outflow radial velocity, Figures III-1 compare the bias and standard deviation of velocity estimates from the spectral differencing and autocorrelation based algorithms . Estimate standard deviations are shown both before and after the spatial smoothing described above. The calculations assume that the outflow velocity is constant from the surface to 100 m height; the radial wind then changes linearly to an "upper level" velocity that is one-third the magnitude of the surface wind and opposite in direction. Reflectivity factor and spectrum width are taken as constant in altitude with values of 40 dBz and 2 m/s respectively. Figure III-2 illustrates this model for a surface outflow velocity of 15 m/s towards the radar.

The velocity estimate performance metrics were calculated using 500 trials of the Monte Carlo signal simulation described in Appendix C. Since essentially all data from our experimental ASR in Huntsville were obtained at a uniform pulse repetition frequency, the simulations here assume a constant PRF of $980s^{-1}$. We show in Appendix C that utilization of the ASR-9's 8/10 pulse alternating PRF waveform would produce only small changes in velocity estimate accuracy. Figures III-1(a) and (b) correspond to a resolution cell where the weather signal to ground clutter ratio is sufficiently large that high pass filtering is not required (Weber, 1987). Part (a) assumes that the resolution cell of interest is at 6 km range and part (b) considers a range of 12 km.

At 6 km range, biases associated with either method are less than 1 m/s. Estimate standard deviations average about 2 m/s before spatial smoothing and are reduced to 0.5 m/s after smoothing. Note that our spectral differencing algorithm (Weber and Noyes, 1988) incoherently averages power spectrum density (PSD) estimates using a running three gate average in range before calculating radial velocity. Thus, more extensive spatial smoothing is required for the spectral

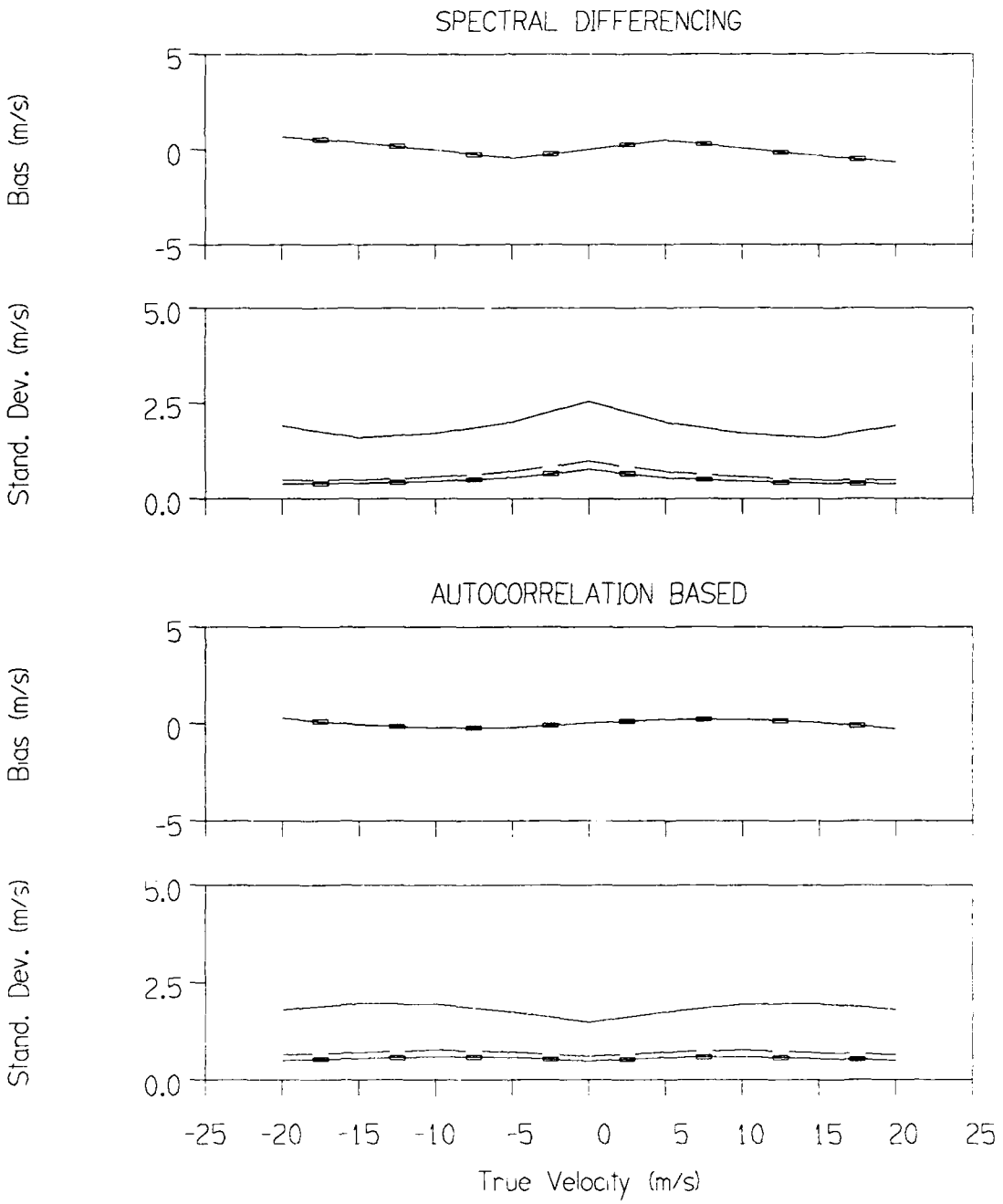

(a) Range of 6 km and no clutter filtering are assumed.

Figure III-1. Spectral differencing and autocorrelation based velocity estimate bias and standard deviation versus "true" outflow velocity. The velocity model of Figure III-2 is scaled proportionally to the abscissae. Solid, dashed and chain dashed curves for standard deviation pertain respectively to single resolution cell estimates, estimates after spatial median filtering and after Gaussian smoothing along the range axis.

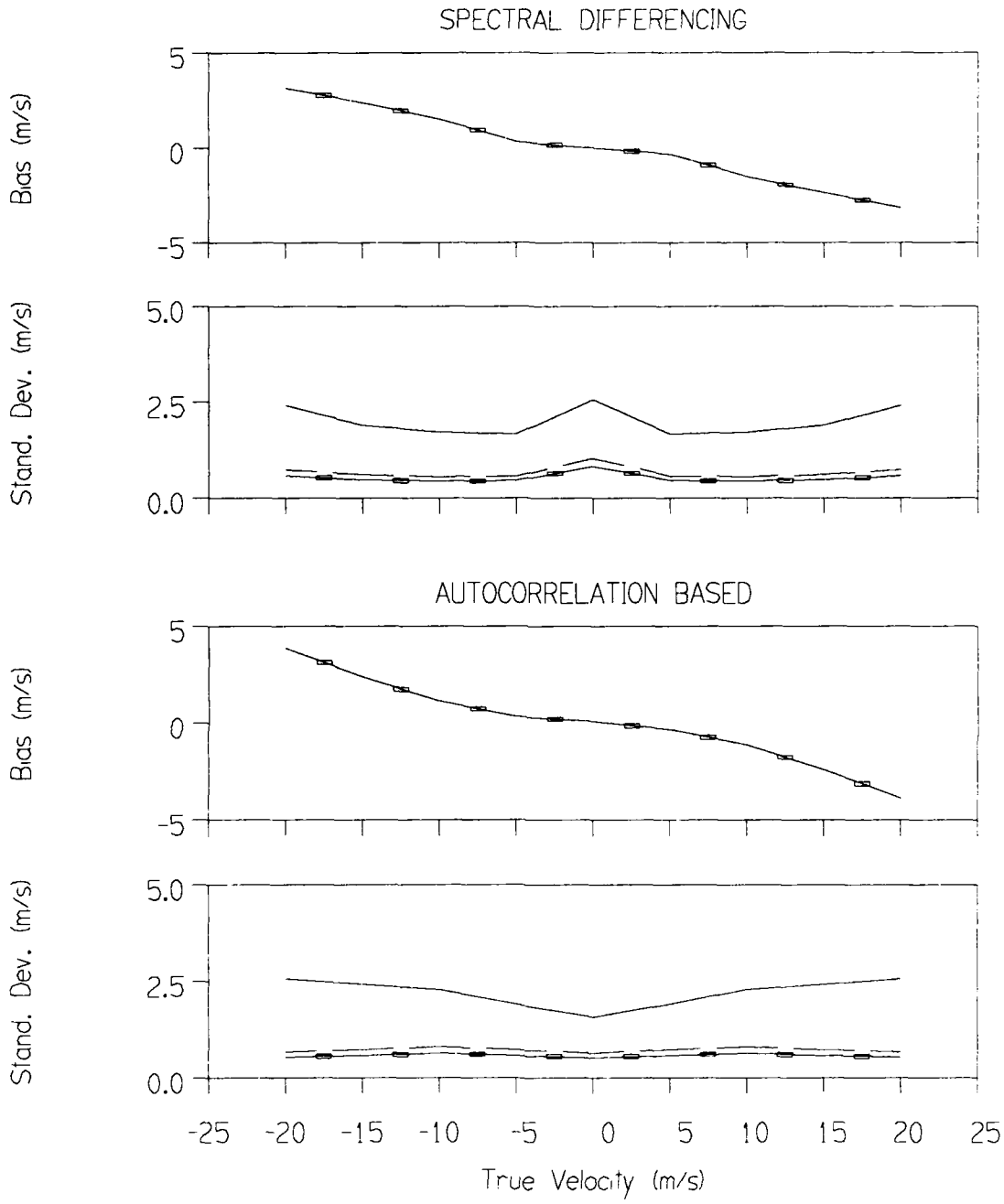

(b) Range of 12 km and no clutter filtering are assumed.

Figure III-1. (continued)

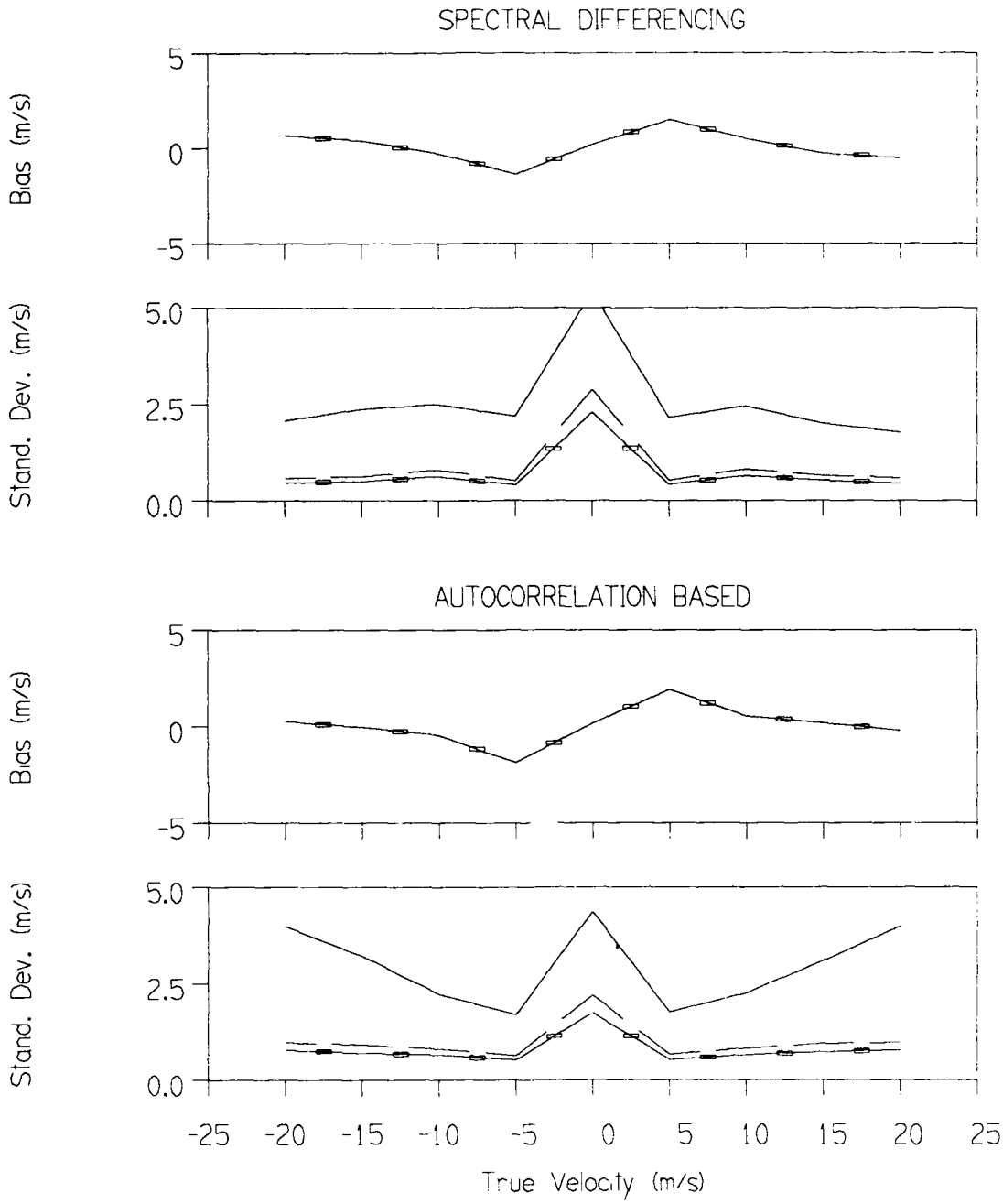

(c) Range of 6 km and use of a clutter filter are assumed.

Figure III-1. (continued)

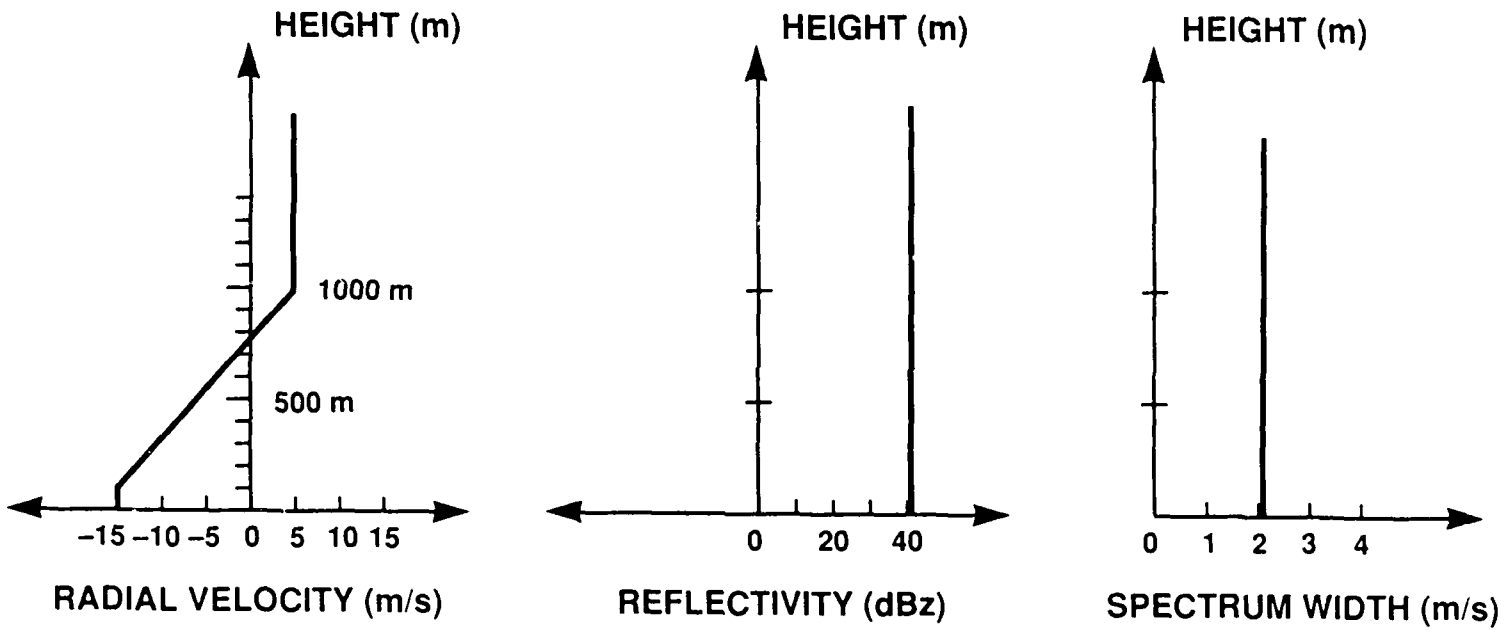

120426-3

Figure III-2. Model vertical profiles of radial velocity, reflectivity and spectrum width in approaching portion of a microburst.

differencing algorithm than for the autocorrelation based method to achieve the stated estimate variance.

Near zero Doppler, the standard deviation of the spectral differencing estimates increases slightly. In our model, there is no vertical shear in the radial wind for zero velocity (i.e. at the microburst center). Without this shear, underlying high and low beam PSDs are the same and the placement in the velocity domain of the low-high beam difference spectrum's positive lobe is governed by statistical fluctuations in the spectral estimates. This lobe -- which is used to generate the low altitude velocity estimate -- can occur anywhere where the PSDs are within a few decibels of their maximum values. This circumstance accounts for the increase in estimate standard deviation at low Doppler. Conversely, for the autocorrelation based algorithm, velocity estimate standard deviations are minimum at zero Doppler where the integrated spectrum width is smallest. This is consistent with Zrnic's (1977) findings that the conventional weather radar pulse-pair mean velocity estimate variance decreases with decreasing spectrum width.

The larger biases at 12 km range (III-1 (b)) represent an underestimate of the surface wind speed; the error increases as surface velocity and vertical shear become larger in magnitude. Maximum calculated bias for the spectral differencing and autocorrelation based algorithms are 3 m/s and 4 m/s respectively. Standard deviations are slightly larger than at 6 km range.

In Figure III-1(c) we repeat the 6 km range calculation assuming that high pass clutter filtering as described by Anderson (1987) or Weber (1987) is required. The filter's stop band width is ±4.7 m/s, providing 39 dB attenuation of scan modulated ground clutter. In addition to removing low Doppler signal power, the 17-coefficient filter reduces the number of valid data points for velocity estimation from 34 to 18. We did not include a ground clutter-induced spectrum component in our signal simulation. Thus, simulated weather spectrum distortion may be larger than would occur with real data where the additional low Doppler power from ground clutter would at least partially offset the filtering.

The overestimate of velocity magnitude resulting from spectrum distortion is maximum when the surface velocity approaches the edges of the filter stop band; at this velocity biases are about 2 m/s for either algorithm. Estimate standard deviations are also large at low Doppler where most of the weather power spectrum lies inside the filter's stop band; even after spatial smoothing, estimate standard deviation would be about 2 m/s for low Doppler signals. At higher Doppler velocities, the effect of the smaller number of available data samples is evident in increased estimate variance relative to the no-filter situation; this increase is more pronounced for the autocorrelation based algorithm. Outside the low Doppler interval however, spatial smoothing is effective in reducing the standard deviation for either method to less than 1 m/s.

Figure III-3 plots velocity estimate bias and standard deviation as a function of microburst reflectivity factor. The calculation used the profile of figure III-2 (surface velocity -15 m/s) except that the reflectivity factor was varied from 30 dBz down to -10 dBz. We assumed a range of 6 km and a sensitivity time control function that places the receiver noise level at an equivalent weather reflectivity factor of 0 dBz (see Weber and Moser, 1987). When the reflectivity factor is greater than 0 dBz, both the spectral differencing and autocorrelation based velocity estimates exhibit minimal bias and standard deviations less than 1 m/s after spatial smoothing. As the signal to noise ratio becomes negative, bias and

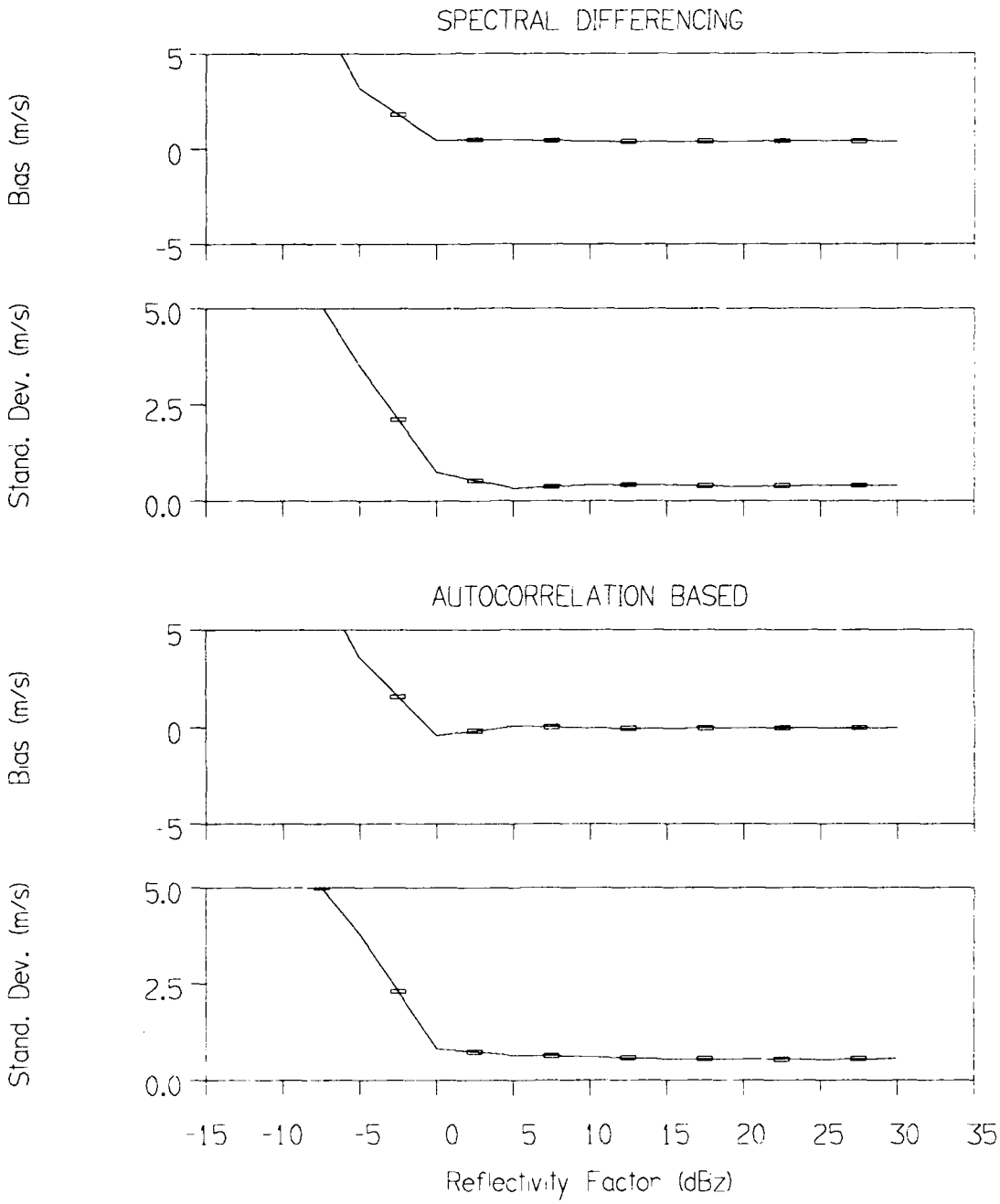

Figure III-3. Spectral differencing and autocorrelation based velocity estimate bias and standard deviation versus outflow reflectivity. The velocity model of Figure III-2 is assumed. The curve for standard deviation pertains to estimates after spatial median filtering followed by Gaussian smoothing along the range axis.

standard deviation increase rapidly. The positive bias reflects the trend of the velocity estimates towards 0 m/s when noise dominates the spectrum. Note that this calculation does not consider the impact of ground clutter. Weber (1987) showed that ground clutter may prevent accurate velocity measurements at short range when the reflectivity factor is less than 20 dBz.

The dependence of velocity estimate accuracy on the vertical extent of the outflow is illustrated in Figure III-4. Here, bias and standard deviation are plotted as functions of outflow height, assuming a range of 6 km. The radial velocity profile is that of III-2 scaled in height by a factor varying from 0.25 to 2.25. The shallowest outflow considered, therefore, has maximum radial winds extending 25 m above the surface and reaches the "upper level" velocity at 250 m. For this height, both algorithms result in significant underestimates of the near surface radial wind magnitude. The bias is 6 and 7 m/s respectively for the spectral differencing and autocorrelation based algorithms. With increasing outflow depth, the bias decreases rapidly to values less than 1 m/s when the outflow layer is 75 m deep. Estimate standard deviation increases by about 50 percent for very shallow outflows.

For Huntsville microbursts in 1987, Weber and Noyes (1988) plotted the distribution of heights at which the radial velocity dropped to half of its maximum value. The median value for this "half-height" was 350 m and about 15 percent of the microbursts exhibited half-heights less than 200 m. These data were compiled from events centered as far as 12 km from the radar where the 3 dB beam width spanned 300 m. Thus, angular resolution may have been inadequate for measuring the actual depths of some of the microbursts. Biron and Isaminger (1989) analyzed RHI scans of microbursts within 8 km of Lincoln Laboratory's 1° pencil beam weather radar. Vertical resolution was therefore 140 m or better. The median half-height for microbursts they measured during 1986 in Huntsville was 400 m; all events were between 300 and 1000 m deep by this measure. For Denver microbursts observed during 1987, the half-height distribution extended from 200 to 1100 m with a median value of 600 m. The median height of maximum velocity in both locales was within the lowest 200 m AGL. For comparison with these statistics, the upper abscissa labels on III-4 give the half-height for the vertical wind profile we assumed in our calculations. At 400 m half-height, estimate bias is less than 1 m/s for either method; the shallowest 15 percent of outflows measured in Huntsville during 1987 would be subject to biases 2.5 m/s or greater at 6 km range.

Radial velocity versus range signatures through a model microburst are simulated in Figures III-5. The basic profile is again that of III-2 but the surface outflow velocity was varied sinusoidally with range and upper level winds were scaled proportionally. Thus the overall structure exhibits surface divergence with compensating convergence aloft as is characteristic of measured microburst wind fields. The model's maximum approaching and receding velocity cores are separated by 2 km. In each plot, the solid line is the "true" surface radial wind pattern; dashed and chain-dashed curves are single realizations of the velocity signature estimated with the spectral differencing and autocorrelation based algorithms.

In III-5(a) and (b) the "microburst" is centered at 6 and 12 km respectively; the upper panels in each figure simulate velocity estimates where no spatial smoothing has been applied. The variance of the unsmoothed velocity estimates disrupts the monotonically increasing pattern between the velocity extrema to the extent

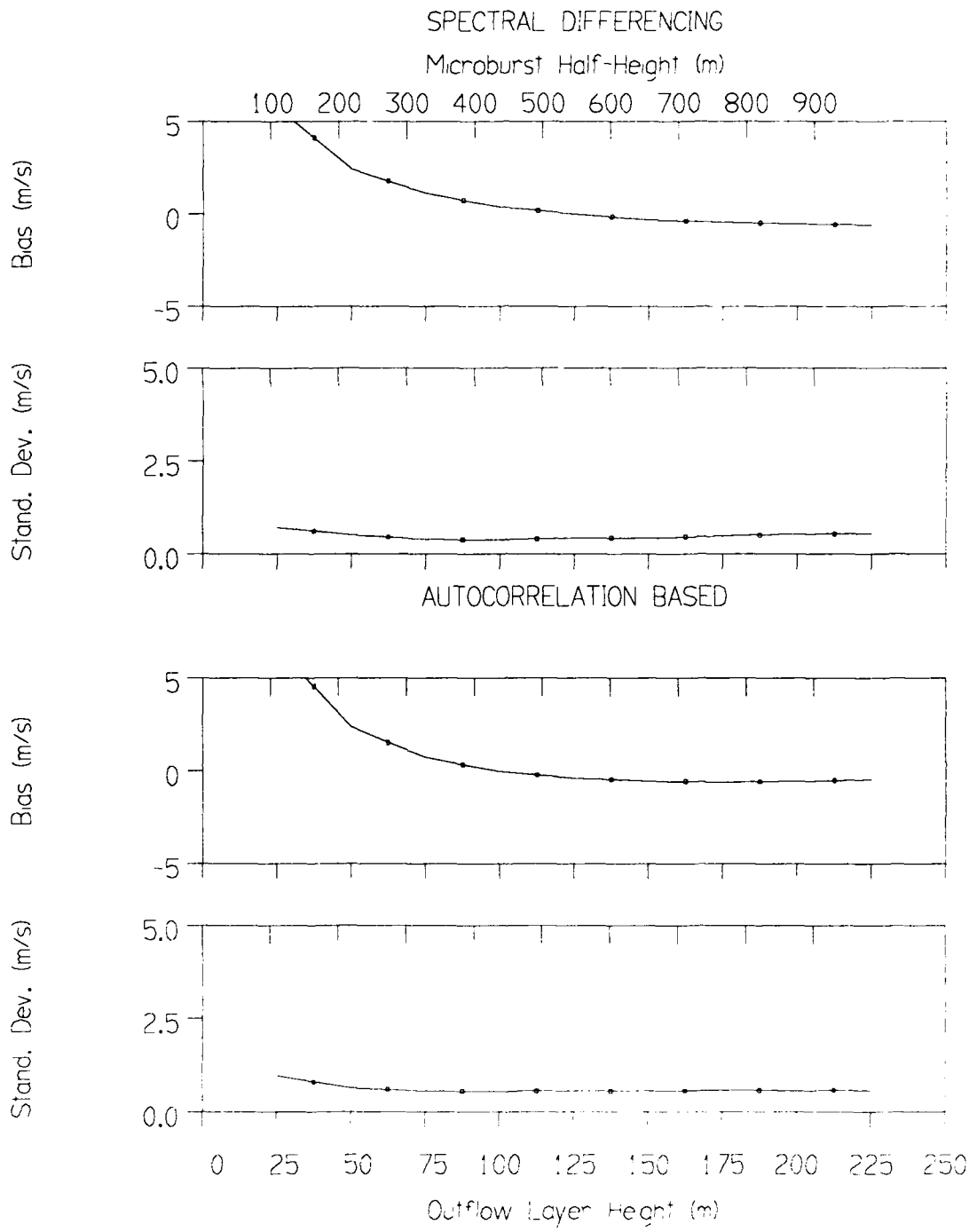

Figure III-4. Spectral differencing and autocorrelation based velocity estimate bias and standard deviation versus outflow height. The velocity model of Figure III-2 is scaled proportionally to the lower abscissa labels. The curve for standard deviation pertains to estimates after spatial median filtering followed by Gaussian smoothing along the range axis.

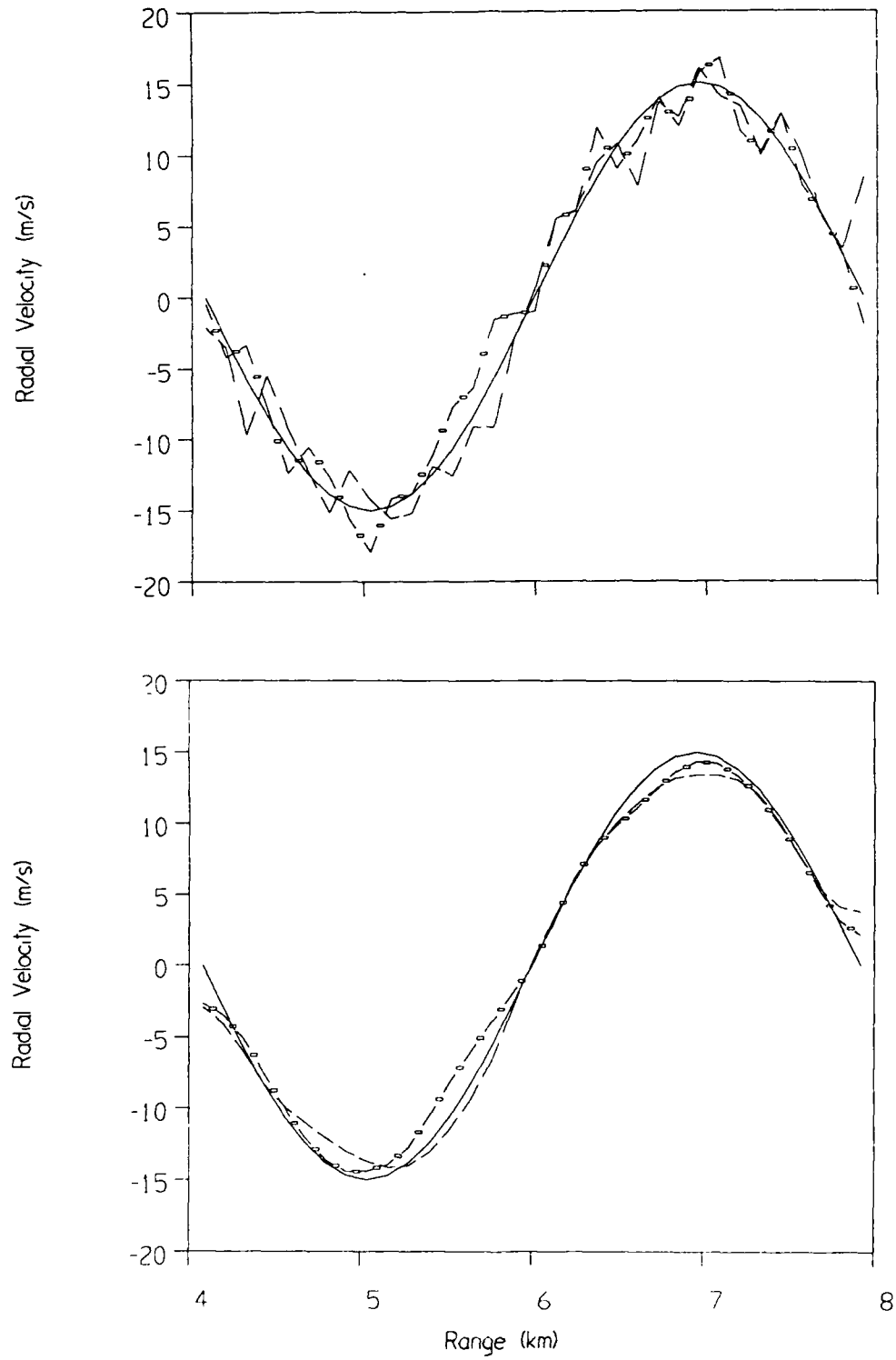

(a) Microburst is assumed to be centered at 6 km range.

Figure III-5. Simulated microburst radial velocity versus range measurements from an ASR. The solid sinusoid is the model for the surface radial wind associated with the microburst. Dashed and chain dashed curves represent estimates using the spectral differencing and autocorrelation based algorithms. The upper plot simulates single resolution cell estimates; the lower plot includes the spatial filtering described in the text.

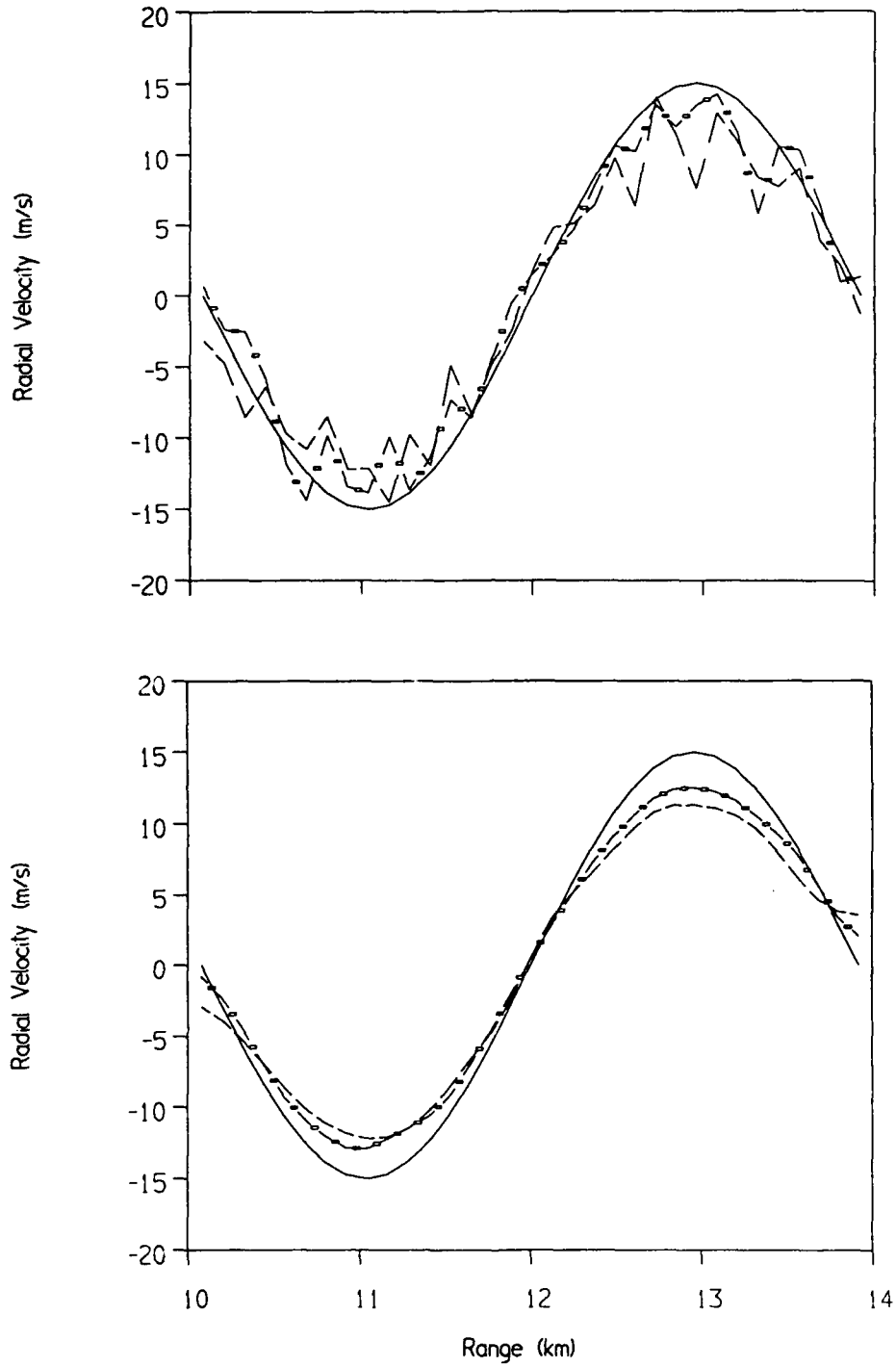

(b) Microburst is assumed to be centered at 12 km range.

Figure III-5. (continued)

that the TDWR microburst detection algorithm might not identify shear segments. The lower panels simulate the spatial smoothing described above. The smoothed velocity fields correlate well with the model wind pattern although the bias indicated in Figure III-1(b) is evident when the microburst is centered at 12 km range.

This simulation based analysis indicates that velocity estimates from the autocorrelation based and spectral differencing algorithms exhibit very similar bias and standard deviation. A representative value for standard deviation after spatial filtering is 0.5 m/s. The most significant factor determining the bias associated with either algorithm is the rate of change of radial velocity with elevation angle. For very shallow microbursts ("half-height" less than 200 m) and microbursts beyond about 12 km range, differential velocity underestimates of 15 percent or more could be expected. However, for the majority of microbursts in the operationally significant region within 12 km of an ASR, our analysis indicates that the accuracy of either velocity estimator is good.

B. Field Measurements from Huntsville Experimental ASR

Lincoln Laboratory's airport surveillance radar weather detection experiment in Huntsville, Alabama during 1987 was described by Weber and Noyes (1988). Equipment and operating procedures during the summer of 1988 were identical except that the scan rate of the C-band pencil beam radar used for "truth" was increased. The basic scan pattern for microbursts in 1988 consisted of two 360° PPI scans at elevation angles of 0.6° and 1.5°, followed by two RHI scans through the outflow. This sequence was repeated at one minute intervals.

Figures III-6 compares images of the radial velocity field estimated from our airport surveillance radar's signals with that measured by the pencil beam weather radar. Data are from a microburst producing thunderstorm on 15 August 1988. The upper left panel is the pencil beam measurement from a scan at 0.6° elevation angle. Two microbursts were present, a strong outflow centered at 10 km range/130° azimuth and a weaker event at 15 km/65°. ASR estimates using the low-high beam spectral differencing technique are shown in the upper right panel with the corresponding autocorrelation based estimate in the lower left. High and low beam signals from the same antenna scan were employed for these estimates. The autocorrelation based estimate obtained when the high beam signal was collected from the following antenna scan is shown in the lower right. For current ASRs, this mode of data collection would be required for operation using circular polarization.

The velocity fields derived from the ASR signals are in good agreement with that measured by the weather radar. In particular the presence of the two microbursts is clearly indicated and the ASR velocity differential estimates are within 1 m/s of the pencil beam measurements. The spectral domain and autocorrelation based wind field estimates from the ASR signals are likewise in good agreement, particularly within the microbursts. Collection of high and low beam autocorrelation estimates on alternate antenna scans (lower right panel) did not significantly change the velocity estimates.

We suspect that the 1.4° beamwidth of the weather radar was too large for accurate measurement of the receding outflow component in the microburst to the southeast. As in some of the other cases presented below, the stronger, more homogeneous receding volume depicted in the ASR-based fields may well be a better representation of the actual wind field.

Additional examples are shown in Figures III-7 through III-9 . In each figure, the upper panel displays the pencil beam radar 0.6° velocity field. The lower left and lower right panels are ASR-based estimates using respectively the autocorrelation and spectral differencing approaches. High and low beam signals were from the same antenna scan since we do not normally transfer data from adjacent scans for analysis.

These examples again indicate good agreement amongst the pencil beam and ASR derived velocity fields. For the displayed scans on 21 June and 25 June, both ASR based velocity differential estimates are within 2 m/s of the pencil beam radar's measurement. The velocity shear estimate from the autocorrelation based ASR field depicted in Figure III-8 is 6 m/s (23%) larger than that derived from the pencil beam radar; the spectral differencing approach resulted in a 3 m/s "overestimate" in this case. Note that the the divergent outflows shown in these examples extend to ranges as large as 20 km (Figures III-8 and III-9).

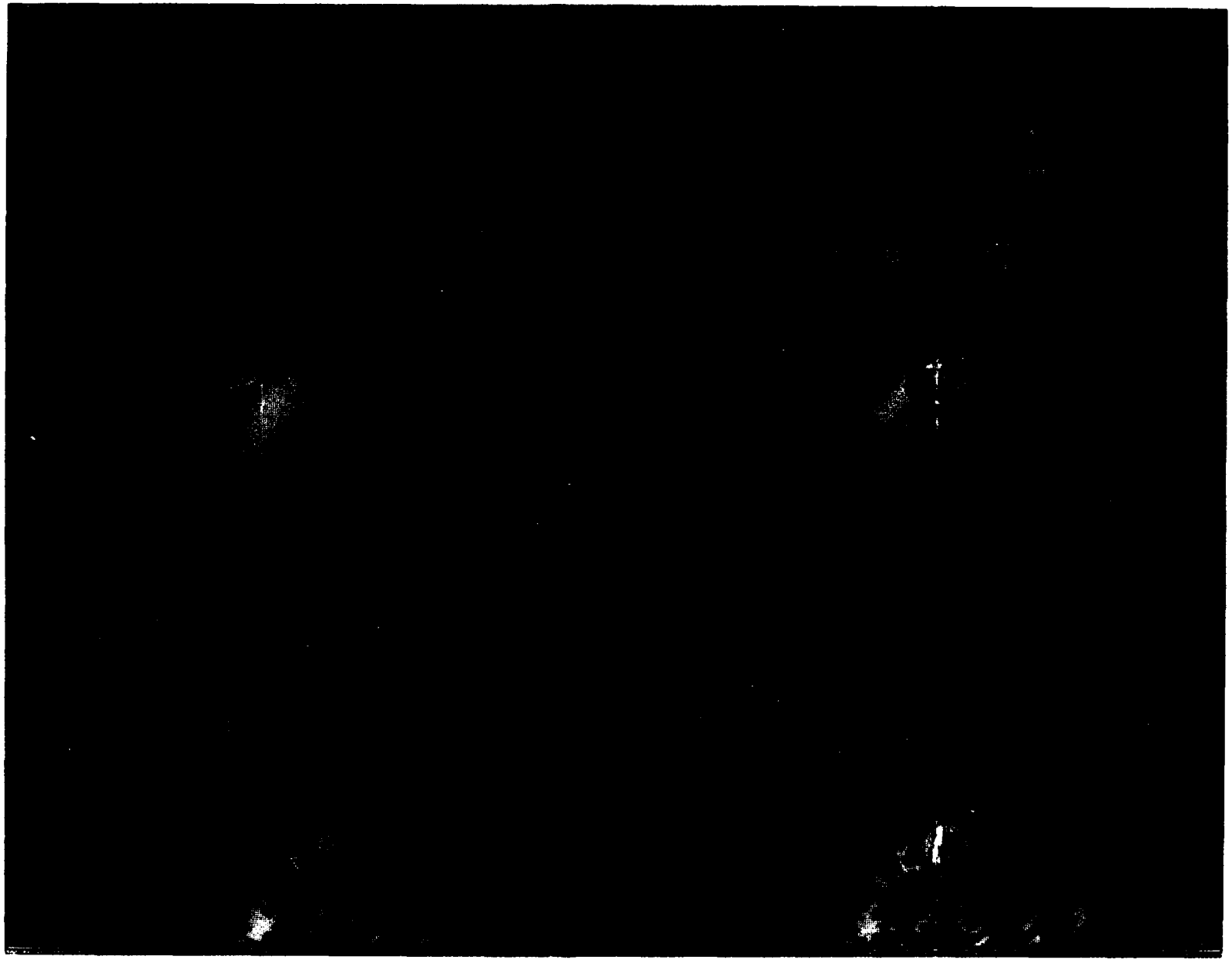

Figure III-6. Images of the radial velocity field in a microburst producing thunderstorm near Huntsville, Alabama on 15 August 1988. The upper left panel shows measurements from the MIT C-band beam weather radar scanning in PPI mode at 0.6° elevation angle. Upper right panel is field estimated from ASR signals using the spectral differencing method. Lower left panel is corresponding field from autocorrelation based algorithm. Lower right panel uses autocorrelation based algorithm and high and low beam signals collected on different antenna scans.

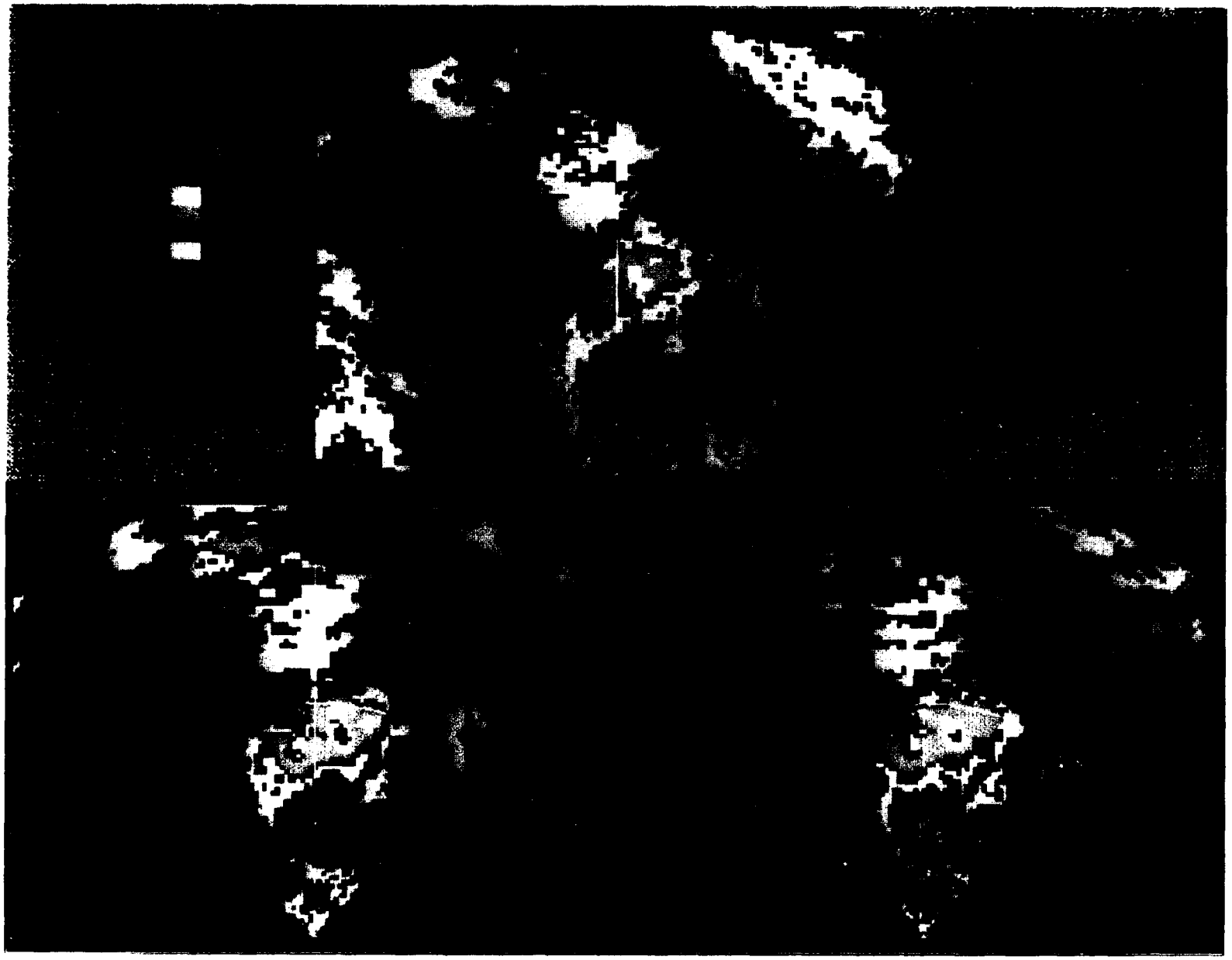

Figure III-7. Images of the radial velocity field in a microburst producing thunderstorm near Huntsville, Alabama on 21 June 1988. The upper panel shows measurements from the MIT C-band beam weather radar scanning in PPI mode at 0.6° elevation angle. Lower right panel is field estimated from ASR signals using the spectral differencing method. Lower left panel is corresponding field from autocorrelation based algorithm.

Figure III-8. Images of the radial velocity field in a microburst producing thunderstorm near Huntsville, Alabama on 24 June 1988. The upper panel shows measurements from the MIT C-band beam weather radar scanning in PPI mode at 0.6° elevation angle. Lower right panel is field estimated from ASR signals using the spectral differencing method. Lower left panel is corresponding field from autocorrelation based algorithm.

Figure III-9. Images of radial velocity field in a microburst producing thunderstorm near Huntsville, Alabama on 25 June 1988. The upper panel shows measurements from the MIT C-band beam weather radar scanning in PPI mode at 0.6° elevation angle. Lower right panel is field estimated from ASR signals using the spectral differencing method. Lower left panel is corresponding field from autocorrelation based algorithm.

A more extensive evaluation of the accuracy of the ASR velocity estimates was derived by "scoring" detections from the TDWR surface outflow detection algorithm against truth as determined from manual examination of the pencil beam weather radar data. The procedure and associated scoring rules are described in Weber and Noyes (1988). Our evaluation utilized approximately 600 scans from the airport surveillance radar in 1988, taken during 35 microbursts on 13 separate days. The scoring was confined to microbursts centered within the operationally significant area extending 12 km from the radar.

Table III-1 summarizes the results of scoring on a scan by scan basis. The listed performance metrics are:

(i) probability of detection -- the number of detected microburst signatures divided by the total number of microburst signatures;

(ii) probability of false alarm -- the number of algorithm alarms not associated with microbursts divided by the total number of alarms;

(iii) bias -- the average difference between ASR-based and pencil beam radar microburst differential velocity estimates. This is expressed both in absolute units (m/s) and relative to the pencil beam radar ΔV_R measurement;

(iv) root mean squared (RMS) difference between the pencil beam radar and ASR-based velocity differential estimates. This equals the square root of the sum of squared estimate bias and estimate variance.

These metrics are tabulated separately for all microbursts and for microbursts with differential velocities greater than 15 and 20 m/s.

TABLE III-1. Microburst detection algorithm performance for ASR-based velocity fields.

Dual Beam Autocorrelation Method

	$\Delta V_R > 10 m/s$	$\Delta V_R > 15 m/s$	$\Delta V_R > 20 m/s$
Detection Probability	0.91	0.90	0.96
False Alarm Probability	0.05	0.04	0.0
ΔV_R Bias (m/s)	2.4	0.9	0.5
Relative ΔV_R Bias	0.19	0.05	0.02
RMS ΔV_R Discrepancy (m/s)	4.8	3.8	3.7
RMS Relative ΔV_R Discrepancy	0.36	0.19	0.16

Low-High Beam Spectral Differencing

	$\Delta V_R > 10 m/s$	$\Delta V_R > 15 m/s$	$\Delta V_R > 20 m/s$
Detection Probability	0.93	0.93	0.97
False Alarm Probability	0.02	0.02	0.0
ΔV_R Bias (m/s)	0.4	-1.0	-1.0
Relative ΔV_R Bias	0.05	-0.05	-0.04
RMS ΔV_R Discrepancy (m/s)	3.4	3.2	3.4
RMS Relative ΔV_R Discrepancy	0.23	0.15	0.14

The results confirm the favorable prognosis for an ASR's capability to detect wet microbursts that we derived from analysis of data collected during 1987 (Weber and Noyes, 1988). Both velocity estimation algorithms supported detection and false alarm probabilities within the 0.9/0.1 bounds called for by the FAA in its TDWR system requirements statement. Over all microbursts scored, the dual-beam autocorrelation method resulted in somewhat reduced detection performance relative to full spectral differencing; detection probability decreased by two

percent while the false alarm probability and discrepancy with pencil beam radar ΔV_R measurements increased. These differences disappeared when scoring was restricted to the subset of microburst scans where the velocity differential exceeded 20 m/s.

Detailed analysis of these data indicates that, for either velocity estimation method, eighty percent of the missed detections were associated with recognizable (by a human observer) divergence patterns in the ASR-based radial velocity field. The automatic microburst detection algorithm did not declare an alarm in these cases because its spatial size and/or continuity requirements were not met (Merritt, 1987). The remaining misses occurred in weak microbursts ($\Delta V_R < 15 m/s$) where the ASR based velocity differential estimates did not exceed the 10 m/s microburst threshold. Our analysis of missed detections does not suggest that divergent outflows are depicted more clearly in spectral differencing versus autocorrelation based velocity fields. Given the subtleties of the automatic microburst detection algorithm, we regard the 2 percent overall difference in detection probabilities using the two velocity estimators as insignificant.

Almost all false alarms occurred in regions where the pencil beam radar measured divergence, but below the required threshold. As seen from Table III-1, autocorrelation based estimates of velocity divergence were larger on average than measured by the pencil beam radar, particularly for weak ($\Delta V_R < 15 m/s$) microbursts. This "bias" produced the higher overall false alarm rate associated with that estimator.

Our simulations (Section III-A) predict that biases, if present, should correspond to underestimates of velocity differential and should be larger for strong microbursts where the vertical gradient in radial wind speed is highest. This is clearly inconsistent with Table III-1. A possible explanation, as alluded to previously, is that the beamwidth and/or ground clutter suppression capability of the pencil beam radar were inadequate for accurate measurement of the strongest, near surface microburst winds. A uniform increase in "true" velocity differential for the 1988 data set would at least produce the expected trend for bias versus microburst intensity.†

Overall, these statistics confirm the previous simulations and case studies indicating that the dual-beam autocorrelation based velocity estimate of equation (3) should support wet microburst detection at approximately the same level of confidence as would be obtained through full spectral differencing. Examination of the storm cases used for the detection performance statistics in Table III-1 is continuing. The analysis will provide more detailed understanding of missed detections or false alarms, and the small differences in detection algorithm performance observed using the two velocity estimators.

† Measured bias for the spectral differencing algorithm applied to our 1987 data set was qualitatively consistent with simulations in Section III-A. Compare for example Figures III-1(b) from this report and the "shear ratio" (i.e. bias) plotted in Figure VI-15 of Weber and Noyes (1988).

IV. DISCUSSION AND FUTURE WORK

The analysis herein confirms our previous assessment that a suitably modified airport surveillance radar would provide an operationally useful capability for automatic detection of "wet" microbursts. In this report, we developed an efficient, autocorrelation based low altitude velocity estimator based on the assumption that the power spectrum of weather echoes measured by an ASR could be adequately represented with a bimodal Gaussian model. Evaluation of microburst detection algorithm performance using the resulting velocity fields indicated that accuracy comparable to the most effective velocity estimator treated by Weber and Noyes (1988) -- low-high beam spectral differencing -- might be achieved with considerable reduction in computational and hardware requirements. The combination of high confidence and computational efficiency make this technique an attractive initial candidate for implementation in our real time wind shear processor.

Ongoing evaluation of ASR velocity estimation techniques will seek to further quantify tradeoffs between accuracy and processing complexity. In addition to the autocorrelation based and spectral differencing methods treated here, we are continuing to assess:

(i) low beam only estimators, for example pulse pair processing following high pass filtering. Necessary front end modifications would be reduced if an ASR wind shear processor only accessed signals from the low receiving beam;

(ii) mapping from the phase of the cross spectral density between low and high beam signals to elevation angle (Anderson, 1989). This technique may produce more accurate near-surface velocity estimates and offers the potential for three-dimensional reflectivity and wind measurements. Note however that high and low beam signals must be accessed simultaneously; thus on current ASRs this method could not be employed during operation with circular polarization.

Each of the candidate algorithms will be scored against all available data from our field experiments in Huntsville and our current site near Kansas City, Missouri. Our goal is to develop reliable performance statistics in order to specify the design of an ASR wind shear processor.

We did not consider here the use of reflectivity factor measurements from an ASR as a supporting and/or precursory indicator of microburst activity. Field measurements with pencil beam Doppler weather radars have shown that descending reflectivity cores frequently presage the development of strong surface outflows (Isaminger, 1988). While temporal growth of the reflectivity field measured by the low beam of an ASR may provide indirect evidence of a descending core, less ambiguous information could be be derived from comparison of reflectivity in "upper" and "lower" beams. The high and low beams could be used directly in this manner although they overlap substantially. Better differentiation would be provided by combining data from the two beams in an effort to explicitly separate received power into upper and lower altitude components. This could be done in the frequency domain using techniques analogous to those described for velocity estimation. Alternately, amplitudes from the dual Gaussian spectral model -- calculated as in the appendices to this report -- could provide the desired reflectivity measures. We are examining the development of the reflectivity field as seen by our experimental ASR to determine appropriate data processing approaches for its use in microburst detection.

As pointed out by Weber and Moser (1987), slightly lower gain and increased "beamfilling loss" for an ASR's high beam reduce sensitivity to low reflectivity weather. This may limit the utilization of dual beam techniques for "dry" microburst and gust front detection. As currently implemented, our dual-beam velocity estimation algorithms compare received power from both beams to receiver noise; if only the low beam signal passes this threshold test, we revert to a standard low beam mean velocity estimate for that resolution cell. Analyses of gust fronts observed in Huntsville and simulation of dry microbursts using volume-scan pencil beam weather radar data are underway to quantify the ability of ASRs to detect low reflectivity wind shear. These will establish firm low-end reflectivity limits for ASR wind measurements.

We noted previously instances where the accuracy of our pencil beam "truth" radar's velocity field was questioned owing to its relatively broad 1.4° beam. Limited clutter suppression capability and slow scanning also reduce confidence in velocity measurements from this radar. To more reliably quantify the accuracy of ASR wind estimation algorithms, we have located our experimental ASR at the same site as Lincoln Laboratory's TDWR test bed. That system will provide a narrower beam (1° in 1989 and 0.5° after conversion to C-band operation in 1990), good clutter suppression and rapid volumetric scanning. The scan strategy facilitates direct comparisons with an ASR's surface wind estimates and understanding of errors through analysis of the three-dimensional wind field. Field measurements will continue in 1990 at Orlando, Florida. Collection and analysis of ASR wind measurements in these varied environments will refine our understanding of the capabilities of ASRs for wind shear detection.

REFERENCES

Anderson, J., *The Measurement of Doppler Wind Fields with Fast Scanning Radars: Signal Processing Techniques,* Journal of Applied Meteorology, 4, pp 627-633, 1987.

Anderson, J., *Techniques for the Detection of Microburst Outflows using Airport Surveillance Radars,* 3rd International Conference on the Aviation Weather System, Anaheim, Ca., January 30-February 3,1989.

Atlas, D., *Radar Detection of Hazardous Small Scale Weather Disturbances,* United States Patent Number 4,649,388, March 10, 1987.

Atlas, D., *The Detection of Low Level Windshear with Airport Surveillance Radar,* 3rd International Conference on the Aviation Weather System, Anaheim, Ca., January 30-February 3,1989.

Biron, P. and M. Isaminger, *High Resolution Microburst Outflow Depth Data from Huntsville, Alabama and Denver, Colorado,* Project Report ATC-163, Lincoln Laboratory, MIT, in press, 1989.

Isaminger, M., *A Preliminary Study of Precursors to Huntsville Microbursts,* Project Report ATC-153, Lincoln Laboratory, MIT, FAA-PM-87-35, 1988.

M.W. Merritt, *Automatic Detection of Microburst Windshear for Terminal Doppler Weather Radar,* Digital Image Processing and Visual Communications Technologies in Meteorology, Cambridge, MA, 26-28 October, 1987.

Sirmans, D. and B. Bumgarner, *Numerical Comparison of Five Mean Frequency Estimators,* J. Appl. Meteor. 14, 991-1003, 1975.

Weber, M. and W. Moser, *A Preliminary Assessment of Thunderstorm Outflow Wind Measurement with Airport Surveillance Radars,* Project Report ATC-140, Lincoln Laboratory, MIT, FAA-PM-86-38, 1987.

Weber, M. *Ground Clutter Processing for Wind Measurements with Airport Surveillance Radars,* Project Report ATC-143, Lincoln Laboratory, MIT, FAA-PM-87-21, 1987.

Weber, M. and T. Noyes, *Low-Altitude Wind Shear Detection with Airport Surveillance Radars: Evaluation of 1987 Field Measurements,* Project Report ATC-159, Lincoln Laboratory, MIT, FAA-PS-88-10, 1988.

Zrnic, D., *Simulation of Weatherlike Doppler Spectra and Signals,* J. Appl. Meteor. 14, 619-620, 1975.

Zrnic, D., *Spectral Moment Estimates from Correlated Pulse Pairs,* IEEE Transactions Aerospace and Electronics Systems, AES-13, pp 344-354, 1977.

APPENDIX A: ESTIMATION OF DUAL GAUSSIAN SPECTRAL PARAMETERS USING $R(\tau)$ and $R(2\tau)$

The first three autocorrelation lags associated with the assumed dual Gaussian spectra in equation (1) are:

$$R_i(0) = a_{i,1}+a_{i,2} \tag{A-1}$$

$$R_i(\tau) = a_{i,1}\exp(-2\pi^2\sigma_1^2\tau^2)\exp(i2\pi f_1\tau) + a_{i,2}\exp(-2\pi^2\sigma_2^2\tau^2)\exp(i2\pi f_2\tau) \tag{A-2}$$

$$R_i(2\tau) = a_{i,1}\exp(-8\pi^2\sigma_1^2\tau^2)\exp(i4\pi f_1\tau) + a_{i,2}\exp(-8\pi^2\sigma_2^2\tau^2)\exp(i4\pi f_2\tau) \tag{A-3}$$

where i=1,2 indexes the low and high beams.

Measurement of $R_i(0)$ and $R_i(\tau)$ provide only six relations for the eight unknown spectral parameters whereas the addition of $R_i(2\tau)$ results in an overdetermined system of equations. We derive therefore a solution based on measurements of the autocorrelation function at lags τ and 2τ. We first eliminate between the two beams in equations (A-2) and (A-3) the autocorrelation function components due to one of the spectral modes. For example:

$$R_1(\tau)-\frac{a_{1,2}}{a_{2,2}}R_2(\tau) = [\frac{a_{1,1}a_{2,2}-a_{1,2}a_{2,1}}{a_{2,2}}]\exp(-2\pi^2\sigma_1^2\tau^2)\exp(i2\pi f_1\tau) \tag{A-4}$$

$$R_1(2\tau)-\frac{a_{1,2}}{a_{2,2}}R_2(2\tau) = [\frac{a_{1,1}a_{2,2}-a_{1,2}a_{2,1}}{a_{2,2}}]\exp(-8\pi^2\sigma_1^2\tau^2)\exp(i4\pi f_1\tau) \tag{A-5}$$

The center frequency f_1 of this spectral component may be determined iteratively by finding the weight $(a_{1,2}/a_{2,2})$ such that the phase angle of equation (A-5) is twice that of (A-4). The phase angle of equation (A-5) may have to be unfolded before comparison to that in (A-4). In performing the search, we make use of the known high and low beam patterns to constrain the possible values of this weight. Our convention is that the first Gaussian component in equation (1) is associated with low altitude winds (below an elevation angle θ_0) and the second with winds aloft. Thus the desired weight:

$$\frac{a_{1,2}}{a_{2,2}} = \frac{\int_{\theta_0}^{\frac{\pi}{2}} Z(\theta)B_1(\theta)B_1(\theta)d\theta}{\int_{\theta_0}^{\frac{\pi}{2}} Z(\theta)B_1(\theta)B_2(\theta)d\theta} \tag{A-6}$$

can be shown to be in the range 0 to 1.0 for reasonable values of θ_0 and the reflectivity factor profile $Z(\theta)$. Here B_1 and B_2 are the low and high beam one-way elevation antenna patterns.

Having determined the weight $(a_{1,2}/a_{2,2})$ the spectrum width σ_1 is calculated by dividing the magnitude of (A-4) by that of (A-5):

$$\sigma_1^2 = \frac{1}{6\pi^2\tau^2}\,\frac{|R_1(\tau)-\frac{a_{1,2}}{a_{2,2}}R_2(\tau)|}{|R_1(2\tau)-\frac{a_{1,2}}{a_{2,2}}R_2(2\tau)|} \tag{A-6}$$

The factor $[\frac{a_{1,1}a_{2,2}-a_{1,2}a_{2,1}}{a_{2,2}}]$ is now readily derived from either (A-4) or (A-5).

An analogous procedure is used to derive the center frequency and width of the "upper level" Gaussian component as well as the ratios $(a_{1,1}/a_{2,1})$ and $[\frac{a_{1,1}a_{2,2}-a_{1,2}a_{2,1}}{a_{2,1}}]$. Four functions of the $a_{i,j}$ have now been determined; from these the values of these amplitudes can be readily determined.

APPENDIX B: ESTIMATION OF DUAL GAUSSIAN SPECTRAL PARAMETERS USING $R(0)$ and $R(\tau)$

We now assume that the two spectral components have intrinsic amplitudes a_j that are modified by known beam weighting coefficients $w_{i,j}$. The weighting coefficients are determined by equating the integrated power of the spectrum in equation (2) with that which would be determined from a known profile of the radar reflectivity factor $Z(\theta)$:

$$\begin{aligned} R_i(0) &= a_1 w_{i,1} + a_2 w_{i,2} \\ &= \int_0^{\frac{\pi}{2}} Z(\theta) B_1(\theta) B_i(\theta) d\theta \qquad \text{(B-1)} \\ &= Z_{1-avg} \int_0^{\theta_0} B_1(\theta) B_i(\theta) d\theta + Z_{2-avg} \int_{\theta_0}^{\frac{\pi}{2}} B_1(\theta) B_i(\theta) d\theta \end{aligned}$$

Note that the radar constant is taken as unity in equation (B-1). The amplitudes a_j are seen to be "average" reflectivities within assumed lower (below θ_0) and upper elevation angle intervals. The $w_{i,j}$ are integrals between the appropriate elevation angle limits of the low or high beam two-way elevation patterns.

The first two autocorrelation lags of the the spectra in equation (2) are given by the first line in (B-1) and:

$$R_i(\tau) = w_{i,1} a_1 \exp(-2\pi^2\sigma_1^2\tau^2)\exp(i2\pi f_1\tau) + w_{i,2} a_2 \exp(-2\pi^2\sigma_2^2\tau^2)\exp(i2\pi f_2\tau) \qquad \text{(B-2)}$$

The six unknown parameters are now the a_j, σ_j and f_j of the two Gaussian spectral components.

The amplitudes a_j are easily computed by applying the inverse of the precomputed beam weighting matrix $w_{i,j}$ to the measured $R_i(0)$. Center frequencies and widths of the two spectral components can be determined by eliminating the other component between the high and low beams in equation (B-2). For example:

$$R_1(\tau) - \frac{w_{1,2}}{w_{2,2}} R_2(\tau) = \left[\frac{w_{1,1}w_{2,2} - w_{2,1}w_{1,2}}{w_{2,2}}\right] a_1 \exp(-2\pi^2\sigma_1^2\tau^2)\exp(i2\pi f_1\tau) \qquad \text{(B-3)}$$

The phase angle of (B-3) determines the center frequency f_1. The spectrum width σ_1 can be determined from the magnitude of (B-3), since the a_j are now known. An analogous procedure can be used to compute f_2 and σ_2.

The important result is that the phase angle of equation (B-3) is proportional to the desired "low altitude" Doppler velocity. The phase angle, however, will be incorrectly computed if the amplitude a_1 is negative. In order that a_1 be positive, it can be shown that $R_1(0)$ must be greater than $w_{1,2}\, R_2(0)/w_{2,2}$ or about 0.6 $R_2(0)$. Owing to the stochastic nature of weather echoes and the limited number of samples available from an ASR for integration, this condition may not be met, particularly if the autocorrelation lags for the two beams are computed on alternate antenna scans. To ensure valid determination of the phase angle, we solve a modified set of equations where the high beam data samples are scaled to have the same integrated power as the low beam. The resulting estimate for the "low-altitude" mean Doppler frequency f_1 is equation (3) in Section II-B-2.

APPENDIX C: SIMULATION OF AIRPORT SURVEILLANCE RADAR SIGNALS FROM MICROBURSTS

The power spectrum, $\tilde{S}$, measured in an range-azimuth cell by a fan beam ASR can be expressed in terms of the elevation angle resolved field of velocity spectra, S, as:

$$\tilde{S}(\phi,R,v) = \frac{\int_0^{\frac{\pi}{2}} S(\theta,\phi,R,v) B_{TR}(\theta) d\theta}{\int_0^{\frac{\pi}{2}} B_{TR}(\theta) d\theta} \tag{C-1}$$

where $B_{TR}(\theta)$ is the two-way elevation power pattern of the ASR antenna. Given either measured or assumed vertical profiles of weather velocity spectra, this relationship can be used to synthesize the power spectrum that would be measured by an ASR.

As an example, Figure C-1 shows power spectra that would be measured in the model "microburst" described in Section III-A. Plots in the left column are for the approaching radial velocity cores and those in the right column are for the receding cores. Center ranges of 3, 6, 9 and 12 km are assumed. Recall that in both cores, the magnitude of the surface radial wind component is taken as 15 m/s (dashed vertical line), decreasing to 5 m/s with opposite sign 1000 m above the surface. The simulations are in good agreement with the bimodal spectrum model assumed in this report. The more complex structure sometimes observed in measured spectra results from vertical wind profiles more complicated than assumed, or from statistical error in the spectrum estimates (see below).

The stochastic nature of radar signals scattered from precipitation can be simulated using a Monte Carlo method proposed by Zrnic (1975) and used by Sirmans and Bumgarner (1975). Equation (C-1) is evaluated on a discrete grid of equispaced frequencies spanning the Nyquist interval. A single realization of the discrete Fourier transform (DFT) of a signal conforming to this spectrum shape is then simulated by multiplying the square root of the spectral lines by randomly generated complex numbers. The amplitudes of these numbers are Rayleigh distributed and the phases are distributed uniformly between 0 and 2π. An inverse DFT then provides synthetic in-phase and quadrature radar signals with the appropriate spectral distribution. Our simulations employed 64-point Fourier transforms, from which the 34 samples required for emulation of the signal processing operations described in the text were extracted.

Simulation of spatial smoothing was accomplished by generating the appropriate number of independent signal realizations. Adjacent range and azimuth gates in real radar data are not fully independent because radar pulse and beam shape create an overlap region where the same scatterers contribute to the echoes. This effect was not simulated and would result in estimate variance slightly larger than our calculations.

Figures C-2 are simulated power spectral estimates for the underlying spectra in Figure C-1. Incoherent averaging of three independent realizations has been performed to reproduce the range averaging applied to our real data. Substantial distortion of the underlying shapes occurs owing to the large variance for power

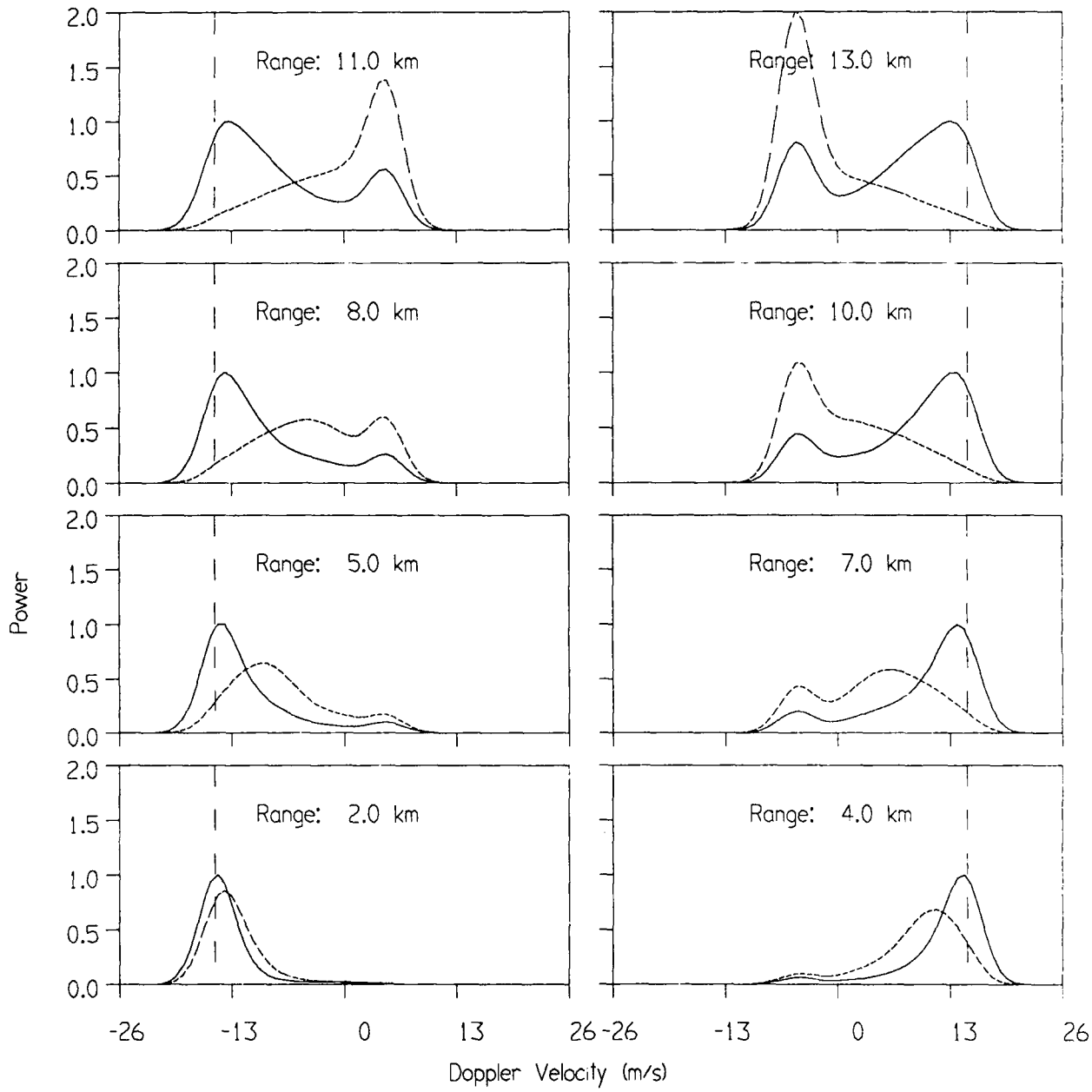

Figure C-1. Simulated underlying ASR power spectra for microburst wind field model of Figure III-2 (and its mirror image). Plot format is as in Figures II-1 and II-2.

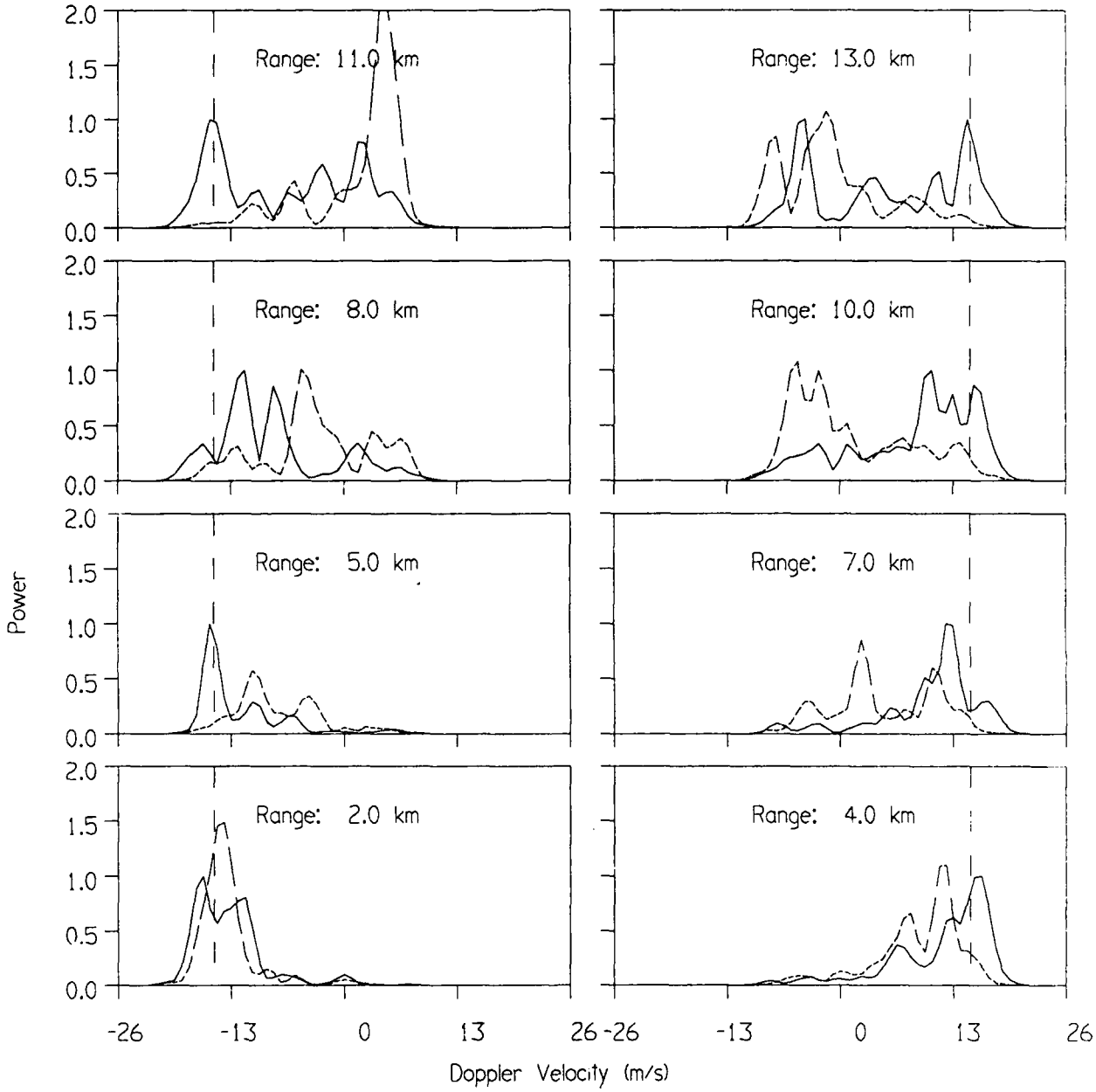

Figure C-2. Simulated three-degree-of-freedom ASR power spectra estimates. Underlying spectra are as in Figure C-1.

spectrum estimates with three degrees of freedom. In general however, the estimate fidelity is sufficient to show the overall width of the spectra and the important low-high beam amplitude relationship in the velocity interval associated with near surface scattering.

Signals from an ASR-9's 8/10 pulse alternating PRF waveform can be simulated by expanding the frequency domain for spectrum synthesis to a value equal to the reciprocal of the largest time increment that is a submultiple of both pulse repetition intervals. After inverse Fourier transformation, the non-equispaced data samples are extracted from the resulting oversampled sequence. Using simulated alternating PRF data, Figure C-3 repeats the calculations of velocity estimate bias and standard deviation shown previously in Figure III-1. As described by Weber (1987), a four-coefficient shift-variant interpolation filter has been used to reconstruct a uniformly sampled data sequence prior to clutter filtering and/or velocity estimation. The bias of velocity estimates would be unchanged by use of the alternating PRF waveform; estimate standard deviation increases slightly relative to the constant PRF calculation. After spatial smoothing, calculated estimate standard deviation varies from 0.5 to 1.0 m/s increasing with range and the magnitude of the true surface velocity. As previously, larger standard deviations apply for low Doppler weather when a clutter filter is used (part c).

Note that the interpolation procedure would break down for weather signals that exceed the Nyquist velocity associated with the lower PRF (about 25 m/s). In this situation, aliasing to different parts of the velocity spectrum would occur at the two PRFs, causing potentially significant spectrum distortion. To prevent resulting velocity estimate errors, tests should be performed on received signal parameters within each PRF block (for example, the first spectral moment) to detect differential aliasing. Appropriate dealiasing procedures could then be applied to the signals prior to velocity estimation.

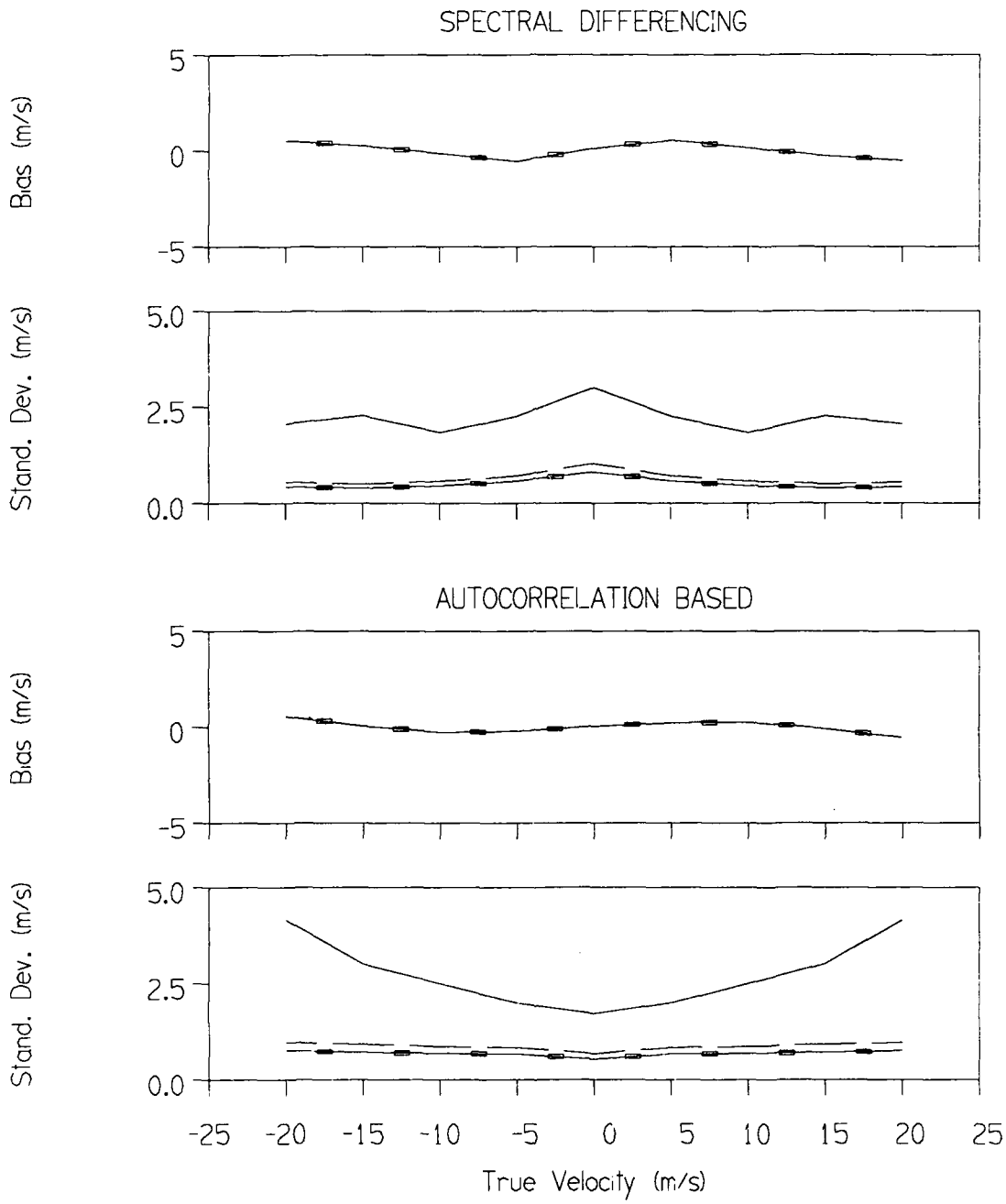

(a) Range of 6 km and no clutter filtering are assumed.

Figure C-3. Spectral differencing and autocorrelation based velocity estimate bias and standard deviation versus "true" outflow velocity. The simulations used here reproduce the alternating PRF waveform of an ASR-9 and the use of a four-coefficient interpolation filter. Plot format is as in Figure III-1.

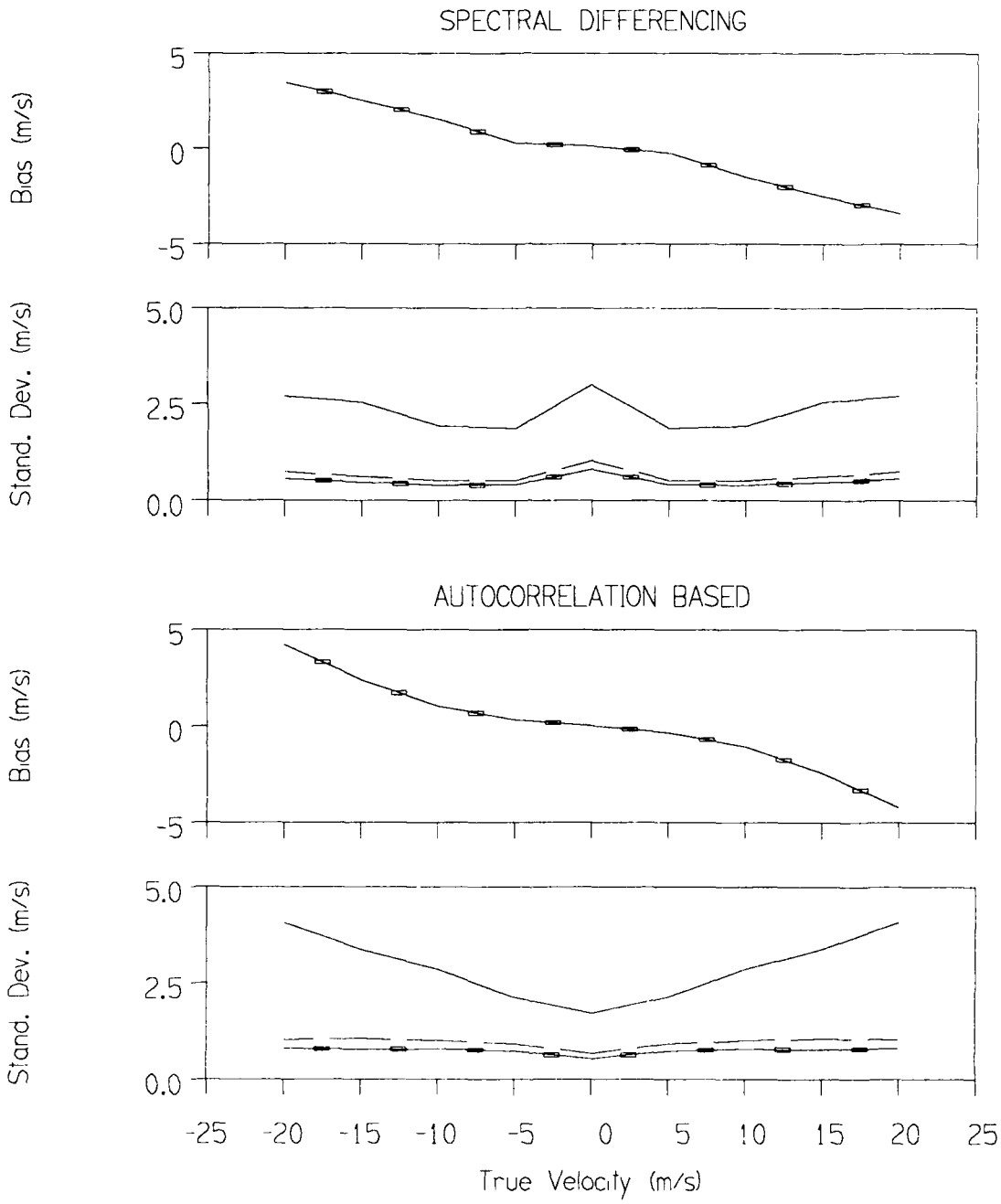

(b) Range of 12 km and no clutter filtering are assumed.

Figure C-3. (continued)

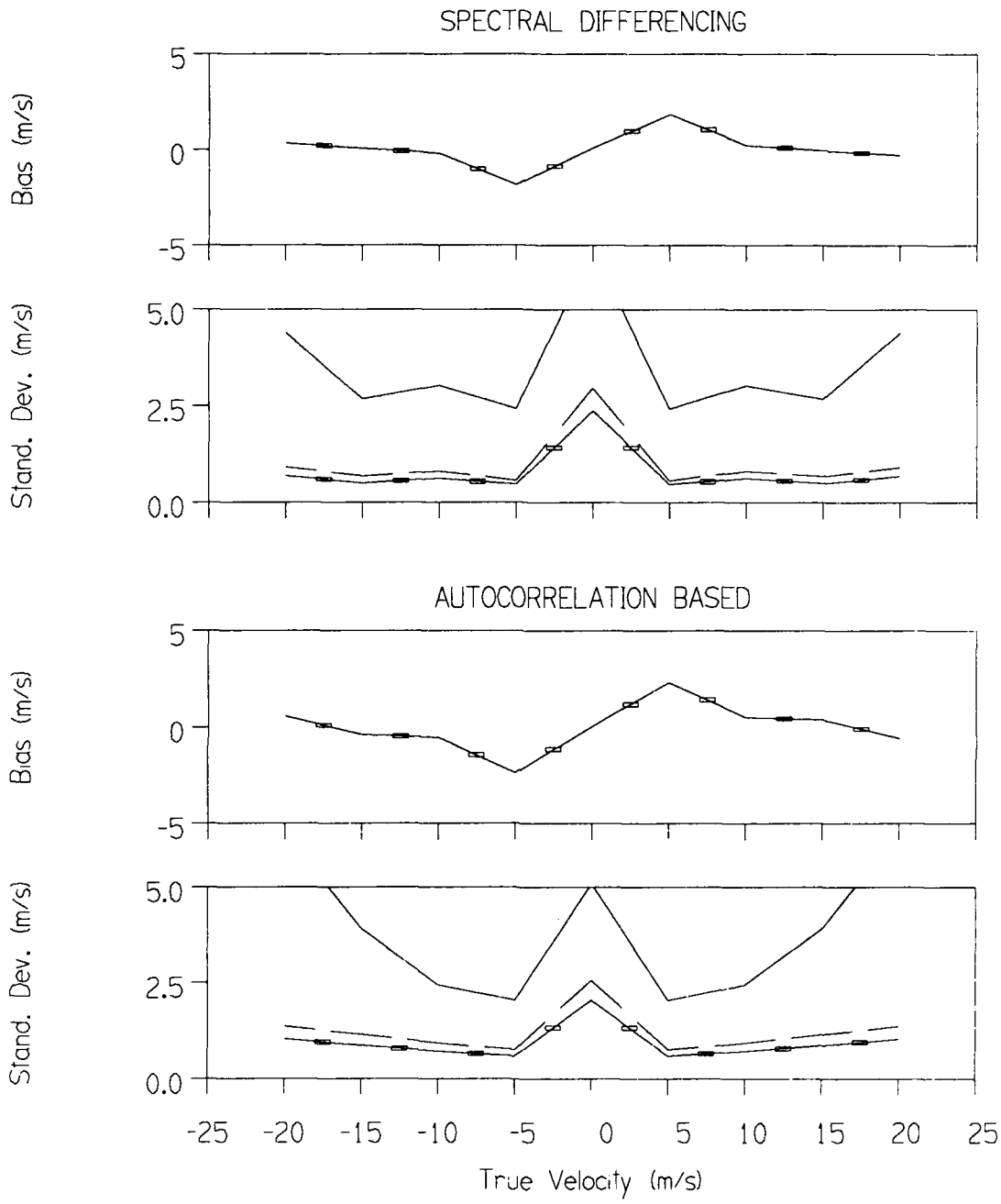

(c) Range of 6 km and use of a clutter filter are assumed.

Figure C-3. (continued)